Università degli Studi di Pavia

Dipartimento di
Ingegneria Industriale e dell'informazione

Scuola di Dottorato in
Ingegneria Elettronica, Informatica ed Elettrica

XXXI Ciclo

Cooperative Indoor Localization under Uncertainties

Ph.D. Candidate:
Moses A. Koledoye

Supervisor:
Dott. Tullio Facchinetti

A.A. 2017/2018

"Per aspera ad astra"

Abstract

Localization of wireless nodes in GPS-denied spaces is being applied in a number of scenarios such as sport teams requiring positioning data for post-match analysis, robot teams carrying out a common task in an indoor environment, among other similar applications. These applications would usually involve a sizable number of participating nodes making scalability a fundamental requirement of the localization setup under the constraints of energy efficiency and position update time. Adopting techniques that are resilient to uncertainties in the deployment region of the nodes is important for the overall accuracy of the setup.

In this work, we focus on a range-based cooperative localization technique where nodes are distinguished as either fixed (anchors) or mobile (tags), and are subject to uncertainties in the environment. Cooperation here implies that the positions of all nodes are computed simultaneously using a joint pairwise distance information while uncertainty refers to any known condition that degrades localization accuracy.

These uncertainties are present in the form of a) missing distance measurements; b) obstacles in the deployment region; and c) stochasticity in measurements for cases where Radio Frequency (RF) signal strength is employed for range estimation. The missing distances may be due to either tags being passive or tags acting as transmitters. For this, we propose a specialized form of Multidimensional Scaling (MDS) that tackles the problem by neglecting tag-to-tag interactions while inferring tag positions directly from those of anchors.

Furthermore, obstacles in the deployment region force signals to travel in nonline-of-sight (NLOS) paths often leading to a lengthening of range estimates. For this, we develop a novel approach that reuses an intrinsic property of anchored MDS to cooperatively estimate NLOS biases in the range estimates. The problem is formulated as a constrained-optimization problem whose solution provides positions with improved accuracy and can be solved by Sequential Quadratic Programming (SQP). The approach works entirely at the application layer and is neither concerned with the probability distribution of LOS/NLOS nor any other a priori knowledge

about the environment. Experimental results show that position errors can be reduced by up to 28% for a set up to 4 fixed and 3 mobile nodes.

In the final discourse relating to uncertainties, we examine lightweight filtering techniques for smoothening Received Signal Strength (RSS) measurements to render them more suitable for range estimation. We formulate the expected values of range (in terms of the Cramér-Rao bound) when estimated directly from raw measurements using an unbiased estimator and compare with range estimates from the filtered measurements. Results show that applying a suitable filtering technique can significantly improve the accuracy of range estimation from raw RSSI measurements.

In the last part of this work, we present an open discussion on design considerations for scalable indoor localization deployments.

Acknowledgments

My father, who willingly emptied his pocket into my head these long years.
My mum, whose frequent calls brought solace during these ‘troublesome’ years.
My sister Ruth, for her kind words and encouragement.
Tullio, who supervised this PhD work and provided mentorship in many other areas outside the PhD work.
Gianluca who has committed time to automating software processes in our lab.
Guido and Daniele, whose suggestions saved reading time and debugging effort.
Luis, who supervised my work while in FEUP and gave insights that opened new grounds for my work.
All of my friends who gave meaning to life outside work: Yilkal, Marco, Zik and others.
God, who kept the space-time continuum stable for long enough to have my PhD work completed.

Contents

List of Figures

List of Tables

Acronyms

AoA Angle of Arrival.

AP access point.

BEKF Biased Extended Kalman Filter.

CDF cumulative distribution function.

COTS commercial off-the-shelf.

CRLB Cramér-Rao Lower Bound.

DV distance vector.

EMA exponential moving average.

GPS Global Positioning System.

IMU Inertial Measurement Unit.

INS Inertial Navigation System.

IoT Internet of Things.

IQR interquartile range.

LIDAR Laser Imaging Detection and Ranging.

LOS line of sight.

MAC media access control.

MDS Multidimensional Scaling.

MDS-A Anchored MDS.

MLE Maximum Likelihood Estimation.

NLOS nonline-of-sight.

PDR pedestrian dead reckoning.

PSD Power Spectral Density.

RF Radio Frequency.

RFID Radio-Frequency Identification.

RMSE Root Mean Squared Error.

RSS Received Signal Strength.

RSSI Received Signal Strength Indication.

RT-ToF Round-Trip Time of Flight.

SLAM Simultaneous Localization and Mapping.

SMA simple moving average.

SMACOF Scaling by Majorizing a Complicated Function.

SQP Sequential Quadratic Programming.

TDMA Time Division Multiple Access.

TDoA Time Difference of Arrival.

ToF Time of Flight.

TWR two-way ranging.

UAV Unmanned Aerial Vehicle.

UWB ultra-wideband.

WSN Wireless Sensor Network.

Chapter 1

Introduction

"*Where in the subway are you now?*"

Anon.

Recent developments in areas such as Internet of Things (IoT) and ubiquitous computing are creating increasing interests in object localization where the position of devices is required for improved interaction between the devices and improved usability for end users [14, 15]. Indoor localization is of peculiar interest in different application areas including guided navigation for visually impaired and self-guided tours at museums [66], augmented reality [77], sports [28], location-aware advertising [5], warehouse navigation [31], and indoor robot navigation [90] among others. In sports, for example, players may be equipped with mobile wireless nodes to enable real-time positioning capabilities for maximizing player performance by helping coaches make better decisions via in- and post-match analysis, enabling early detection of player injuries and assisting referees with the enforcement of the rules of fair play. In applications related to robotics, robots may be shipped with localization capabilities that allow real-time tracking of their location during a remote operation in a Global Positioning System (GPS)-denied environment, say in a tunnel, allowing remote control or easy pickup at the robot's known location whenever human intervention is required. In other commercial applications, objects in storage can be fitted with passive devices (e.g. Radio-Frequency Identification (RFID)) that can relay triggers or become activated when the objects are moved past certain points, effectively ensuring the continuous storage of the objects in a safe location and preventing theft. The nature and peculiarities of the specific application dictate the form of the adopted localization system, which might vary from cheap and low energy wireless devices to costly high-resolution camera positioning systems.

The wide interest on indoor localization is further proved by the Microsoft Indoor Localization Competition, a yearly competition that assesses indoor localization

Figure 1.1: Microsoft Indoor Localization Competition, CPS Week, Porto 2018.

solutions from different teams around the world highlighting the strength and weaknesses of their various approaches and rewarding the best performances with cash prizes [62]. The results of the yearly competitions served as a continuous benchmark for our work considering different metrics and helped to keep track of state of the art challenges in indoor localization. Figure 1.1 is an image of the competition organizers and some of the teams setting up their solutions.

1.1 An Overview of Indoor Localization Systems

Indoor localization involves the estimation of location from physical properties of the environment that change from point to point, such as RF signal intensity, RF time of arrival, ultrasound signal intensity, ultrasound time of arrival, magnetic field intensity and other sensory information such as visual features. The aforementioned properties or features can be used individually or combined to improve the accuracy of a localization system. The various technologies that enable the estimation of location using some of the aforementioned properties are discussed in the following sections.

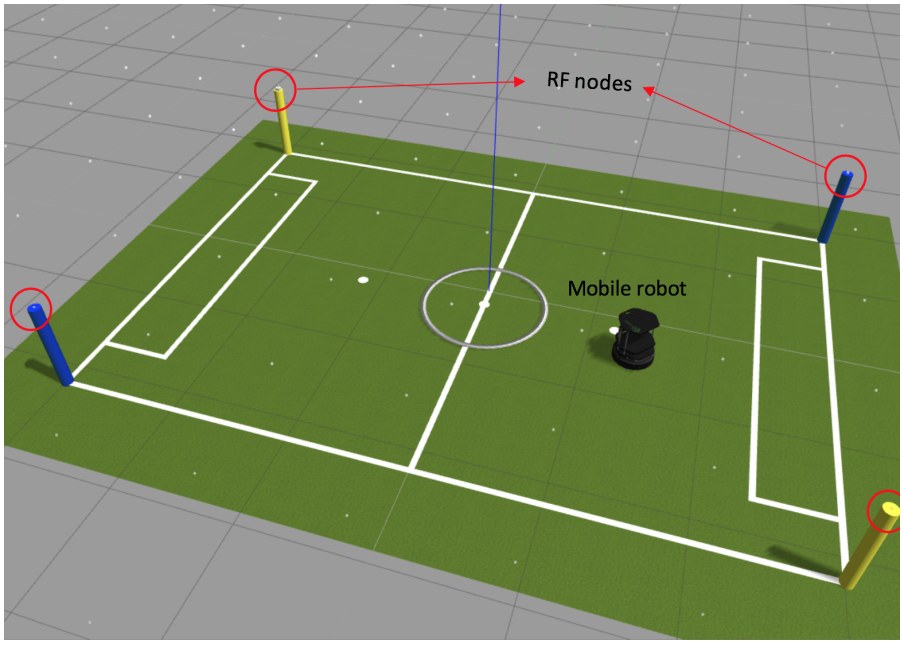

Figure 1.2: Simulated RF positioning of mobile robot using four fixed nodes on a small soccer field.

1.1.1 Radio Frequency positioning

In the following, we enumerate and discuss the most common RF-based ranging techniques. For context, a typical deployment of an RF positioning setup with fixed RF nodes at four corners of a rectangular boundary and a mobile robot fitted with RF communication capabilities is shown in fig. 1.2.

1. Received Signal Strength (RSS) decreases with distance giving an indication of the proximity of the receiver's antenna to the transmitter's, allowing to roughly estimate an approximate location for the receiver with respect to the transmitter. The RSS path loss model expresses the mathematical relationship between distance, power at the receiving antenna, and reference power at a known distance from the transmitter [75]. To utilize this model, knowledge of a channel constant which parameterizes the traveled channel is required. This constant is known as path loss exponent. RSS is very suitable due to its simplicity and the readily available RSS measurements from existing wireless devices [106]. RSS measurements might express relatively high variance at long range due to the increased likelihood of reflections, occlusions and interference in the deployment region of the RF devices, otherwise, the variance is fairly constant with distance [74].

2. Time of Flight (ToF) compared to RSS is more commonly used due to its higher localization accuracy. Since the speed of radio signals in free space is a known constant, given the time of travel, distance can be estimated using the standard velocity-time-distance relationship. Thus, the estimation of distance relies on the assumption that the path traveled by the signal is entirely in free space and that it is a straight line. However, this is not always the case, as RF signals can be occluded or reflected by obstacles in the deployment region of the RF nodes.

   Moreover, while ToF promises high accuracy, it requires highly specialized hardware to compute signal travel time which is usually in the order of tens of nanoseconds for a few meters; an error of a few tens of nanoseconds will lead to large inaccuracies in the distance estimation. ToF can be combined with RSS for improved localization performance [32]. To further improve accuracy by reducing effects of measurement noise, ToF can be collected for round trips between transmitter and receiver yielding Round-Trip Time of Flight (RT-ToF). RT-ToF is mostly suitable for cases where RF receivers are passive [92].

3. Time Difference of Arrival (TDoA) is a similar time-based measurement that is applicable to synchronized receiving antennas. The antennas at different positions receive the signal at different time instances and by extension different points in the signal phase. All the time difference equations can be put into a system of linear equations and solved to compute the range of the transmitter from each receiver or compute directly the position of the transmitter. The accuracy of TDOA measurements improves with the distance separation between the receivers because this increases the time difference between the arrival times [33].

4. Angle of Arrival (AoA) measures the direction of travel of a signal as seen from an antenna array [83, 52]. This direction can be determined from TDoA measurements for the individual antennas in the antenna array. In other cases, rotational antennas can be used and the direction that yields the maximum signal strength is deemed the direction of line-of-sight propagation of the signal [13]. This angle can be used to compute the location of the transmitting device. One clever application of AoA is its use for determining the location of a caller when antennas are geo-localized at the same base station.

The aforementioned techniques are all affiliated with range-based positioning. For RF based range-free positioning, existing infrastructure such as Wi-Fi routers and

beacons are used to coarsely estimate location. Wi-Fi RSS fingerprints from different known locations are collected in a database to be used afterward with k-nearest neighbor or a neural network for inferring the location of a new RSS measurement.

1.1.2 Ultrasound positioning

Ultrasound positioning uses properties of ultrasound – sound waves that operate at high frequencies not audible to human hearing – for location estimation. The techniques used are similar to those of RF: time of flight and signal strength, where transmitters and receivers are swapped with sound emitters and microphones respectively [45] and as with RF, ultrasound ToF is the more commonly used. Ultrasound ToF positioning is however more accurate than that of RF because ultrasound travels much more slowly, allowing the corresponding hardware to measure the time more precisely[35], although echo effects are a major drawback. In less common applications, ultrasound RSS can be used to provide coarse location estimates by checking if an audio signal is audible within a range or not.

1.1.3 Magnetic positioning

Magnetic positioning systems use local variations in earth's magnetic field to provide localization capabilities. They are relatively easy to set up as they usually do not require additional hardware other than magnetometers which most smart phones are already shipped with. In recent applications, the magnetic field intensity variations across different positions are stored to be used afterwards with new data to check the closest match [95]. However, since these variations are influenced by large metallic objects, the displacement of these objects might render an old database of magnetic field intensities across the area useless; consider for example an escalator or lift operating in the vicinity of the fingerprinted area, whose motion can significantly change the magnetic levels in the environment of interest. To improve the signal to noise ratio, artificial magnets with high strength can be placed at known locations to redefine the magnetic signature of the deployment area [87].

1.1.4 Camera-based positioning

Positioning systems that use cameras rely on visual features or markers to track object position and are known for relatively high accuracies. In the more common use cases, a database of features at different locations in the environment is collected, which is afterwards used to match new images from a camera to determine the

location of the camera. An example of this is a landmarked based positioning system for persons who are visually impaired [4].

Applications requiring higher accuracies would require more than one camera and depend on computer vision algorithms to determine the location of tracked objects. These objects are usually easily distinguishable from other objects in the environment, such as players with numbered jerseys in a basketball game. The main drawback of camera-based positioning systems is the failure of such systems under poor visibility.

1.1.5 Inertial measurement

Inertial measurements collected from Inertial Measurement Units (IMUs) composed of gyroscopes and accelerometers are used to update the position of an agent via dead reckoning. The IMU device is mounted on the object of interest, so that its linear acceleration and angular velocities are captured, and the path traveled by the object can be approximately constructed. Most often, IMUs also include magnetometers so the object's heading can also be captured. Since IMUs only track motion rates, the initial position of the object must be known before IMU measurements can be used to determine new positions. As such, inertial measurements are seldom used alone, and are instead used as part of more elaborate localization techniques such as radio positioning [64], Simultaneous Localization and Mapping (SLAM) [51] or GPS navigation [49].

1.2 Cooperative Localization

The problem of cooperative localization involves assigning each object in a given $N \times N$ matrix of pairwise distance measurements to N points in a p-dimensional metric space such that the distances between the points match as closely as possible the distances in the given matrix. The participating nodes work together in a peer-to-peer manner to collect measurements [74]. Thus, under cooperative localization, the accurate localization of one node is coupled with the localization accuracy of every other node with which the initial node shares information. Accurate localization of one node might imply a near accurate localization of the other nodes, and a degraded localization accuracy of a node would easily suggest a poor localization accuracy rippling to other nodes. Each node requires a minimum of three connections with other nodes in a 2D setup. Issues that contribute to accuracy loss are the same as those in a non-cooperative context and are discussed briefly in section 1.3. Increasing

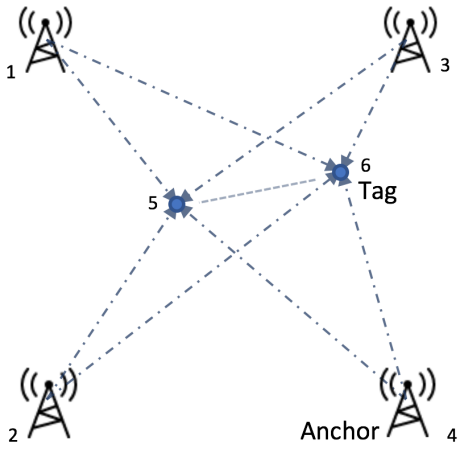

0	d_{12}	d_{13}	d_{14}	d_{15}	d_{16}
d_{21}	0	d_{23}	d_{24}	d_{25}	d_{26}
d_{31}	d_{32}	0	d_{34}	d_{35}	d_{36}
d_{41}	d_{42}	d_{43}	0	d_{45}	d_{46}
d_{51}	d_{52}	d_{53}	d_{54}	0	d_{56}
d_{61}	d_{62}	d_{63}	d_{64}	d_{65}	0

Figure 1.3: Inter-node ranging between mobile and fixed nodes, intra-node ranging between mobile nodes and the final matrix of pairwise distances.

the number of nodes in the deployment area is one way to increase the overall accuracy in a cooperative localization setup.

A typical set up of a cooperative localization scheme where the pairwise distances between all nodes are known is shown in fig. 1.3. From fig. 1.3, the nodes are distinguished based on their mobility: a) fixed nodes are known as anchors; b) mobile nodes are known as tags. The adjacency matrix in the figure is a matrix showing the pairwise distances between all nodes in the setup. Diagonal elements – i.e., distance of a node from itself – are zero, while the distances between anchor nodes $d_{ij},\ \forall i, j \in [1, 4]$ are constant.

1.3 Open Issues in Indoor Localization

Indoor localization is an evolving field as new solutions and techniques are constantly being developed to meet challenges of every day life that use localization in one form or another. Nevertheless, there are existing issues that require innovation in order to make current localization solutions more usable for real tasks in uncontrolled environments. Some of these issues will be highlighted in the following paragraphs and are all addressed later on in this work.

Improved accuracy of indoor localization systems can speed up adoption of such systems in the same way GPS or similar satellite positioning technologies have received mass adoption. While some approaches have reported centimeter and decimeter level accuracies [96, 55], such level of accuracy is yet to be reported in

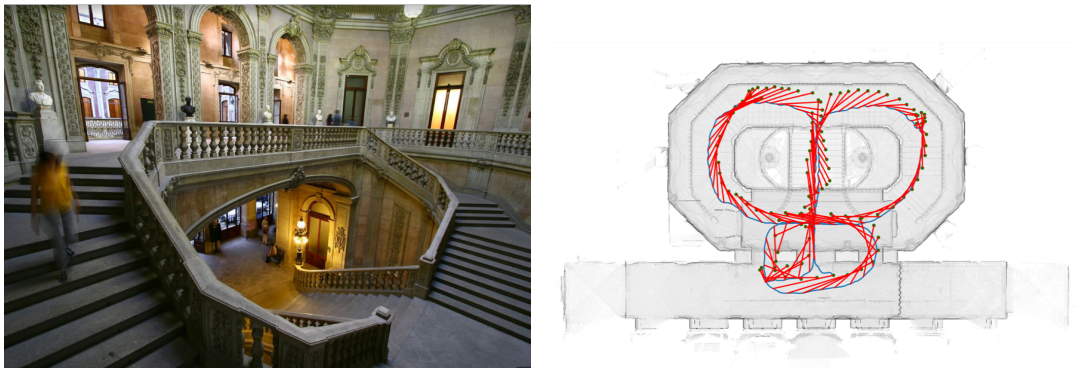

(a) Localization exercise at Palácio da Bolsa stairway.

(b) 2D category first place result with 2.4m mean error.

Figure 1.4: Microsoft Indoor Localization Competition 2018 results (see footnote 1).

most practical test scenarios. Moreover, cost intensive approaches that meet this level of accuracy such as Laser Imaging Detection and Ranging (LIDAR) systems might be impracticable from an economic, ergonomic and scaling point of view.

Going by the results of the 2018 Microsoft Indoor Localization competition, the best results in the 2D and 3D categories reported average error values of $2.4m$ and $0.27m$ respectively[1]. A plot of the localization performance of the best result in the 2D category alongside a picture of the stairway are shown in fig. 1.4. The 3D category had better performance as the evaluation space is a 3D one – the main stairway at Palácio da Bolsa (see fig. 1.4a). More so, both results can be considered optimistic as the evaluation tests were carried out in open space where some of the equipments had a clear line of sight. Apparently, accuracy improvements in uncontrolled and unfamiliar environments is one area that still requires a substantial amount of input.

A resilience to the effects of environmental variables, which largely relates to accuracy, affects the stability of the performance of indoor localization systems. Such effects are due to the dynamics of the environment which can degrade the performance of a localization system e.g. reflection or occlusion of signals, blockade of camera visibility, change in signature of magnetic field intensity. In this work, we focus only on resilience to nonline-of-sight (NLOS) effects in the context of range-based localization.

Setup time and the man hour requirements for deployment is another area which if improved can impact significantly the adoption of indoor localization solutions. Solutions should be easy to deploy with little technical expertise if they are to reach and become usable by a much larger audience. A reuse of existing infrastructure

[1]These results are available on the competition website.

or infrastructure free solutions can also greatly reduce setup time or the technical know-how required.

Localization systems that can work under incomplete information about the environment are also very desirable. The more reason why approaches that require substantial amount of information about the environment or its agents (which might include the localization system itself) are less suitable when compared to the alternatives e.g. building a database of RF or magnetic fingerprints in the environment is hardly sustainable in a fast paced work place. In our work, we consider the case where the ranging information shared between nodes required for good cooperative localization is incomplete.

Other issues such as privacy and compliance with government regulations are more societal than technical, and are therefore considered as issues beyond the scope of this work.

1.4 Research Questions

With the aforementioned open issues, we present the following research questions that this thesis is posited to address:

1. Do cooperative localization algorithms present an advantage over other classical localization methods in the presence of uncertainties?

2. In the presence of incomplete information and NLOS effects, can cooperative localization algorithms be reformulated to still provide accuracies within the $1m$ benchmark?

3. By how much are uncertainties likely to impact the performance of a localization exercise?

4. By how much can the accuracy of ranging be improved given a collection of statistical methods that can be applied for preprocessing?

5. What are the likely bottlenecks that can impede the scaling of our selected cooperative localization algorithm?

With these in mind, we proceed to state quantitatively the contributions of this thesis.

1.5 Contributions

To tackle accuracy problems resulting from NLOS effects in the environment, we developed a novel cooperative algorithm for mitigating these effects. The algorithm, which was originally tested in an RF-based setup, is extensible to any range-infrastructure-based localization system. This cooperative NLOS mitigation algorithm was presented in the following publications:

- M. A. Koledoye, T. Facchinetti and L. Almeida,"Mitigating effects of NLOS propagation in MDS-based localization with anchors," IEEE International Conference on Autonomous Robot Systems and Competitions (ICARSC), 2018, pp. 148-153.
- M.A. Koledoye, T. Facchinetti and L. Almeida, "Improved MDS-based Localization with Non-line-of-sight RF links," Special Edition, Journal of Intelligent and Robotic Systems, 2018, Springer (**under review**).

Handling incomplete data, more specifically, interaction between tags, was addressed by developing a specialized form of an existing cooperative localization algorithm that undermines such missing data. This approach has been shown to outperform another approach that attempts to approximate/predict the missing data. Our specialized form was presented in the following publication:

- M. A. Koledoye, T. Facchinetti and L. Almeida, "MDS-based localization with known anchor locations and missing tag-to-tag distances," 22nd IEEE International Conference on Emerging Technologies and Factory Automation (ETFA), 2017, pp. 1-4.

Later in our work, we compare ranging results of an easy-to-deploy commercial off-the-shelf solution to a customized hardware solution that promises higher accuracy but not without some hardware programming expertise. Under the scope of this comparison, we study different techniques for preprocessing RSS measurements from commercial off-the-shelf (COTS) devices so that the measurements are more meaningful and useful for ranging. Results of the evaluation of the studied preprocessing techniques benchmarked against expected range value when estimated by an unbiased estimator from raw RSS measurements were published in:

- M. A. Koledoye, D. De Martini, S. Rigoni and T. Facchinetti, "A Comparison of Received Signal Strength Indication (RSSI) Filtering Techniques for Range-based Localization," 23rd IEEE International Conference on Emerging Technologies and Factory Automation (ETFA), 2018, pp. 1-7.

1.6 Organization of the document

The rest of the thesis is organized as follows:

- **Chapter 2** opens with background information on indoor localization and then gives an overview of related work citing relevant literature to examine the strengths and weaknesses of existing approaches.
- **Chapter 3** opens with a discussion of cooperative localization, specifically, metric multidimensional scaling as applicable to object localization. An analytical solution to the formulated cooperative localization problem is introduced and a specialized form is provided for cases where distance information in the proximity matrix is incomplete. Results are validated with simulations.
- **Chapter 4** expands on the analytical results in chapter 3 to accommodate NLOS cases in a matrix of pairwise distances with incomplete information. A constrained optimization problem is formulated whose solution yields object positions with higher accuracy under NLOS conditions. Results are validated with simulations and experiments.
- **Chapter 5** gives a summary of lightweight RSS filtering techniques and how the estimated range from each filtered output compares to others and to the expected range value when estimated from raw RSS by an unbiased estimator. Results are validated with experiments.
- **Chapter 6** is an open discussion about the design of cooperative indoor localization systems and their scalability.
- Finally, conclusions on our work are drawn in **chapter 7**.

Chapter 2

Background and Related Work

"Science is what we have learned about how to keep from fooling ourselves."

Richard Feynman

In this chapter, a background on the existing work on cooperative localization and more generally indoor localization, alongside related work in the form of relevant publications are discussed. The related publications cover the contribution areas of this work (highlighted in chapter 1 section 1.5) in order to understand the state of the art prior to our work and give more perspective on the significance of the results of the present research. Our contributions were made at different points of the localization stack described in section 2.1. We start with a general overview of various indoor localization solutions in both cooperative and non cooperative contexts. We focus on RSS and ToF techniques as those are the most applicable to this work.

Localization systems are designed and implemented with careful consideration of trade-offs between accuracy and ease of deployment. Accuracy largely depends on the underlying feature exploited for location estimation, and unlike GPS, there are various possibilities for indoor localization (see section 1.1 for an overview) most of which are RF-based in the form of RSS, signal travel times or angle of arrival. RSS-based localization services although relatively less accurate are widely in use due to their relatively low deployment cost and availability of RSS values on most mobile devices. RSS alone does not satisfy the requirements for fine-grade localization as demonstrated by the accuracy results in [98]. Therefore, using RSS alongside other techniques is quite common practice. For cooperative localization with RSS, [21] proposed a combination of RSS with an Inertial Navigation System (INS), similar to the approach in [109], where an extended Kalman filter is used to fuse both inertial and RSS measurements; the RSS measurements are used to estimate distance/range,

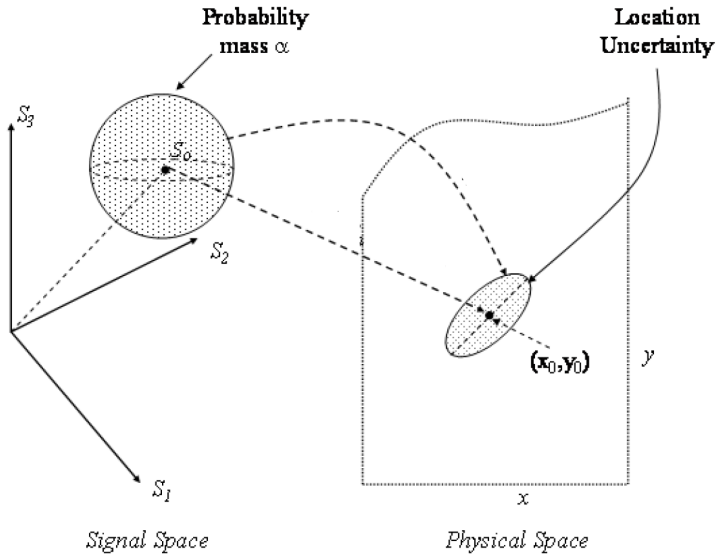

Figure 2.1: Mapping RSS measurement uncertainties to location uncertainties [65].

an exercise commonly referred to as access point (AP) localization.

Methods fusing RSS and ToF combine the efficiency and poor performance of RSS measurements with the more accurate but resource-consuming ToF measurements [40, 32, 63, 72]. Further improvements in accuracy were reported in [105] as the solution adds efficient map matching and an improved motion model to the earlier Kalman filter approaches. On the other hand, RSS if not used directly in the localization algorithm can be used to plot confidence regions for ToF-based (or any other precise scheme) localization where signal strength uncertainty is mapped to location uncertainty as described in fig. 2.1. The signal space hypervolume is computed from the probability mass α which is an incomplete gamma function [56]. This hypervolume maps to an ellipsis in the location space centered on (x_0, y_0).

Standalone applications for RSS also exist where WiFi fingerprints are collected for known points and are used with a learning algorithm for inferring location given new fingerprints [25, 70, 110, 60]. One disadvantage of fingerprinting is the man-hours required to build a database of fingerprints. We performed a cursory Wi-Fi fingerprinting exercise covering our robotics laboratory (see fig. 2.2) which overall required a full working day. While the accuracy can go as low as 1m depending on the granularity of the fingerprints and multiple mobile nodes can reuse one database in a cooperative localization context, the results are only consistent for as long as environment remains unchanged. Displacing a large object from one point to another

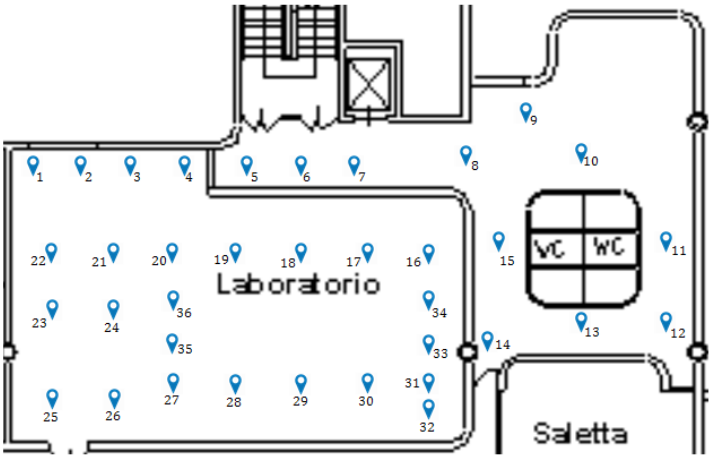

Figure 2.2: Fingerprint points on floor map of the robotics lab.

in the area or human movements can degrade the performance of this localization technique.

ToF on the other hand is much more suitable for commercial grade indoor localization applications compared to RSS. Since ToF requires real time communication between nodes, performance is necessarily dependent on the sampling rate [50] and the underlying scheduling mechanism. Multi-hop routing used alongside Time Division Multiple Access (TDMA) as proposed in [71] is used to improve end-to-end to delays for large teams of collaborating robots, and can be easily extended to cooperative localization for reducing latency and allowing for higher sampling rates. For tracking applications, ToF can be fused with pedestrian dead reckoning (PDR) to improve localization performance [82] where ToF measurements compensate the divergence of PDR measurements, and PDR measurements compensate outlier ToF measurements.

2.1 The Localization Stack

The localization stack consists of different connected components, end-to-end, that interact to provide localization functionality. An overview of a typical localization stack as related to our work is shown in fig. 2.3. As presented in the figure, nodes might be distinguished into two categories based on their mobility: mobile nodes or tags, and fixed nodes or anchors, where mobile nodes measure their positions with reference to fixed nodes. The node labels in the figure are specified with categories since either anchors or tags can transmit their data to a sink device where the data is processed and plotted. An example of a setup where tags localize themselves

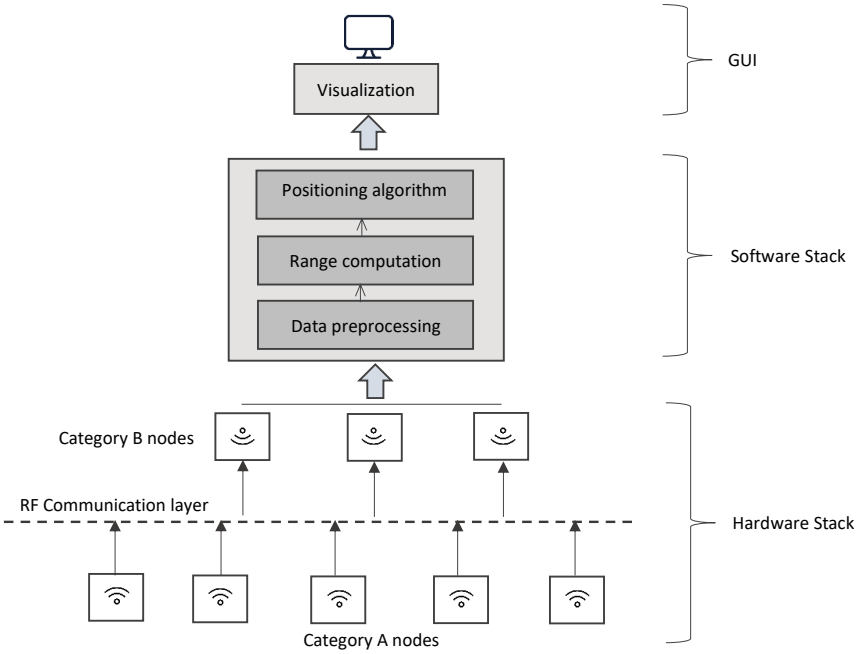

Figure 2.3: The localization stack: hardware, software and GUI components.

w.r.t. anchors and then transmit to a sink is the nanoLoc localization solution [1] which was used extensively in this work. Background work relating to the various components of the stack are discussed in the next sections.

2.2 RF Communication in WSNs

In radio positioning, the communication environment is referred to as the channel. The channel permits the transmission of signals between the participating nodes, sometimes referred to as motes, in the localization scheme. While the localization performance in a Wireless Sensor Network (WSN) depends on the number of anchor nodes within range, it equally depends on the properties of the channel such as channel capacity, bandwidth and the underlying modulation scheme. The choice of various RF communication models in WSNs have been discussed extensively in [65, 18, 6, 58]. Of the various models, the most applicable standards at the physical and media access control (MAC) (a subset of the datalink layer) layers are the IEEE 802.15.4 standard – designed for higher precision ranging and localization capability, the IEEE 802.11 – the most widely used wireless computer networking standard and other IEEE 802.15.x standards. These standards are employed in

narrowband and UWB radios for WSNs as discussed in the following sections.

2.2.1 Narrowband Radios

Narrowband radios refer to RF radios that communicate in channels with a narrow range of frequencies. They have long been used in applications requiring reliable links in different environments as opposed to higher data rate applications. Since the bandwidth required is relatively smaller and the noise floor is significantly lower, the energy required for transmitting signals is equally small [6]. This makes narrowband radios very suitable for low power applications. Narrowband 802.15.4 radios, for example, can turn on their radios, transmit full packet, receive acknowledgment and shut down all in about 5ms [65]. For IEEE 802.11 devices, the power management scheme is managed by the MAC layer of the protocol stack and maintains power efficiency at moderate data rates. However, the limited bandwidth of narrowband radios increases the susceptibility of these radios to multipath effects – moving a narrowband transceiver by a fraction of a wavelength (approx. 12cm at 2.4GHz) will cause the receiver to perceive a supposedly new multipath environment [65]. Direct path and NLOS signals are mostly indistinguishable by the receiver due to this limited bandwidth. This makes narrowband radios less desirable in WSNs where nodes have fast paced dynamics.

2.2.2 UWB Radios

UWB radios utilize pulses that have very short duration that give them ultra-wide spectrum and due to their low PSD cause very little interference with existing narrowband systems [73]. Figure 2.4 shows a plot of PSDs of narrowband and UWB systems. They were developed partially to improve ranging capabilities of radio positioning and as such have the ability to provide highly accurate localization results [108, 57]. The prevailing defining characteristic for UWB signals is that the fractional bandwidth B_f is greater than 0.2. The fractional bandwidth B_f is expressed mathematically as

$$B_f = 2 \cdot \frac{f_H - f_L}{f_H + f_L} \tag{2.1}$$

where f_H and f_L are the higher and lower -10dB bandwidths respectively. Additionally, according to the US FCC rulings, a signal is classified as UWB signal if the bandwidth is greater than or equal to 500MHz [73]. The larger bandwidth allows for higher resistance to multipath effects [100] since direct path and multipath signals are well spaced at the receiver and the earliest path can be the deemed the

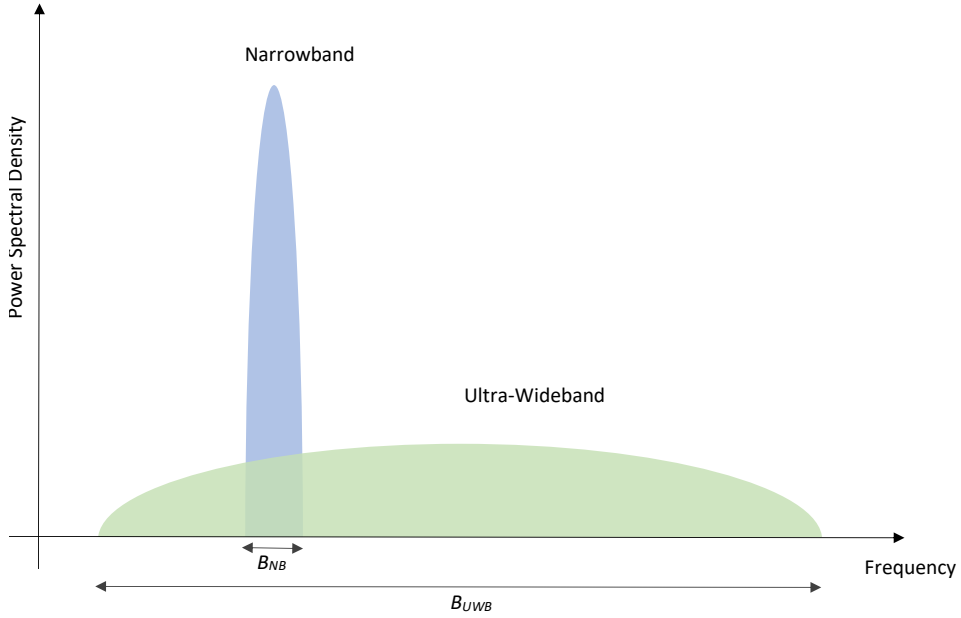

Figure 2.4: PSDs of narrowband and UWB signals.

direct one. More so, the higher data rates in UWB systems can allow them to scale more quickly with regards to data exchange in cooperative networks. IEEE 802.15.4a standards addresses the power efficiency issues with UWB radios which were a major concern in the early adoption of UWB for WSN applications.

2.3 Localization Algorithms in WSNs

Wireless sensor networks can select from a variety of algorithms and techniques for the localization of their component nodes depending on the architecture, use case and required accuracy from the localization exercise. The vector of range measurements for N nodes $\boldsymbol{r}_N$ is related to the locations $\boldsymbol{X}$ by the following equation:

$$\boldsymbol{r}_N = \boldsymbol{g}(\boldsymbol{X}) + \boldsymbol{e} \tag{2.2}$$

where $\boldsymbol{e}$ is the vector of measurement errors and in metric spaces, the mapping function $\boldsymbol{g} : \mathbb{R}^{N\times 2} \rightarrow \mathbb{R}^{N\times N}$ gives the Euclidean distance for a 2-dimensional space defined for any two nodes at points $p \in \boldsymbol{X}$ and $q \in \boldsymbol{X}$:

$$g_{p,q} = \sqrt{(x_1 - x_2)^2 + (y_1 - y_2)^2}.$$

The task of the localization algorithm is to find an optimal set of positions $\hat{\boldsymbol{X}}$ that reproduces as closely as possible the given set of range measurements $\boldsymbol{r}_N$; an inverse

of the expression in eq. (2.2). In a scenario where the distribution of measurement errors f_e is known, the problem can formulated as a maximum likelihood one:

$$\hat{\boldsymbol{X}} = \arg\min_{X} \left\{ \log f_e \left(\boldsymbol{r}_N - \boldsymbol{g}(\boldsymbol{X}) \right) \right\}. \tag{2.3}$$

However, the error distribution f_e is not always known. Nonetheless, one desirable property of localization algorithms in WSNs is that they are able to assess the quality of the range estimates and incorporate that information in the localization process [65]. Localization algorithms that are useful in cooperative contexts are as follows:

1. Distance vector (DV)-hop and DV-distance [69] where messages are propagated from fixed nodes to mobile nodes and on to other anchor nodes hop-by-hop and the hop counts are used to determine distances between hops since anchor to anchor distances are known. A mobile node is therefore able to estimate its position given communication with at least three anchors. DV-distance extends this idea by replacing hop counts with measured inter-node distances.

2. Multidimensional Scaling (MDS) [85, 84] where configuration of points are estimated in a 2 or 3 dimensional Euclidean space given a matrix of pairwise distances between nodes.

3. Linear programming [23] where the localization problem is formulated as a convex optimization problem and solved using linear programming where optimal positions minimize the convex problem.

4. Stochastic Optimization techniques such as simulated annealing [48] and basin-hopping [94] where advanced optimization techniques are used to escape local minimas.

In our work, we use MDS. The main motivation for this choice is due to the extensive existing research that MDS has and its plethora of implementations – classical MDS [59], MDS-MAP(C) and MDS-MAP(P) [85], RangeQ-MDS [61], MDS-A [30], MDS-RFID [88] and MDS-Hybrid [2] among others. These helped gain a wealth of a priori insight allowing to understand what parts of a novel implementation can be tweaked to cover for uncertainties. More so, large node deployments can enjoy from distributed computing since an implementation for running MDS in patches (a subset of MDS-MAP) already exists. We therefore focus on strategies and techniques for positioning under uncertainties as applicable to MDS in the rest of this section.

2.3.1 Positioning under NLOS

The complete removal of NLOS effects and measurement noise may be impossible due to incomplete knowledge about the environment and the nature of obstacles. However, the removal of some amount of NLOS bias and noise from distance measurements has been investigated under various localization contexts that use RF. The more common NLOS mitigation techniques [11, 38, 39, 42, 43, 93, 103, 104] use the propagation channel model or channel statistics from historical data to distinguish between line of sight (LOS)/NLOS signals, in which NLOS ones are detected by identifying some anomalies in the signal property with differentiated values for direct and non-direct paths. Other methods for distinguishing NLOS signals from LOS ones examine the fitness of the various distance measurements under a specified cost function and may employ a priori probabilities about the distribution of NLOS-prone nodes in the deployment area. Methods described in [97] and [102] are applicable to localization algorithms that compute positions on a per tag basis, unlike MDS that computes all positions jointly. The work in [102] presented comprehensive approaches where new distances and bias values are estimated from the original distance measurements via a minimization problem whose performance can be improved by a priori probabilities. A Sequential Quadratic Programming (SQP) based formulation and a Maximum Likelihood Estimation (MLE) where both introduced. Bias was estimated on a per anchor basis with the advantage of reducing the complexity of the minimization problem, and the disadvantage of penalizing the accuracy of NLOS bias estimation. Moreover, the minimization problem was formulated per tag, so that a separate minimization is performed for each tag, leading to likely scaling issues. In a similar related work [81], the authors tune the elements of the covariance matrix R of a Biased Extended Kalman Filter (BEKF) with respect to NLOS identification; matrix elements are increased if NLOS is detected or decreased otherwise. Since their approach is used alongside trilateration, it also does not scale well. Furthermore, their approach works considerably better for setups with a few number of NLOS distances compared to LOS ones. When NLOS measurements are dominant, a scarcity of LOS measurements may lead to estimation failure.

2.3.2 Missing Tags Interaction

Various solutions have been proposed for handling missing data in distance matrices containing pairwise distances of nodes. [85, 84] run the MDS computations in multiple patches for locally connected nodes and then build a global map from the patches. In [26], the authors describe a solution with bounded errors that decrease at a rate

of $\sqrt{n}$, where n is the number of nodes in the region of deployment. A closely related work that uses anchors is MDS-RFID [88] which estimates the missing tag-to-tag distances using a triangular method that takes the sum of the distances of two tags from a given anchor as an upper bound and the difference of the distances of these tags from the anchor as a lower bound for the missing distance. They further propose an averaging method using all available anchors that improves the accuracy of the recovered distances. The previous methods require a preprocessing step to recover the missing information. The accuracy of the estimated configuration therefore depends on the quality of this recovery. In the method we propose later in this work, we avoid the extra computational load of reconstructing the missing data, and still provide an accuracy that betters or matches that of the aforementioned method.

2.4 Data Preprocessing

RF signals possess noisy characteristics usually observable from signal strength fluctuations that can degrade the accuracy of a localization exercise. Preprocessing of the measurements can help put them in better form before they are passed on to the localization algorithm. Location uncertainty values have been shown to decrease due to preprocessing [101] which provides an initial lowering of the variance of the measurements.

2.4.1 RSS Preprocessing

Methods that use RF signal strength exploit a value which is usually measured on most devices as RSSI which corresponds to some value of RSS in `dbm`. This RSSI value is an indication of the power of a received signal as it travels from transmitter to receiver through a propagation medium.

Conventionally, RSS decays with distance and as such gives an indication of the proximity of the receiver's antenna to the transmitter and can therefore be used to roughly infer an approximate distance for the receiver with respect to the transmitter. However, unlike ToF, range estimation using RSS measurements are less accurate since distance estimation is a secondary use of the measurements. More so, the range information RSSI provides is asymmetrical – one may confidently infer close proximity to a transmitter with a high RSS value, but a low value would not necessarily imply that the transmitter is far away [12]. The limitations of RSS and its suitability for localization have been discussed broadly in [44] while the use of the Bluetooth technology (used partly in this work in the comparison of ranging accuracies) for indoor localization has been discussed in [46].

With the obvious pitfalls of RSS, it continues to remain relevant for use in localization [47, 72, 75, 7]. This is mostly because the use of RSSI does not require installation of additional hardware for environments that are already fitted with RF routers. And also because localization with RSSI scales better than those with say ToF since the setup does not require scheduling of transmission time for nodes, and multiple receivers can read their respective RSSI values for a single transmission simultaneously. For the aforementioned reasons, RSSI has experienced continuous use in the indoor localization context. The most common use given large sensor network deployments is in range-free localization where predictive models are used to estimate the location of nodes given a set of RSSI measurements in a database of fingerprints [99, 67, 34, 8]. In range-based localization, the raw RSSI measurements are usually preprocessed before they are passed on to the position estimation algorithm. In [72], for example, a moving median filter was used to smoothen RSSI measurements before they were passed to a Kalman filter that fuses the RSSI measurements with ToF measurements. In [24], a moving average filter was used instead for smoothening, before measurements were used in the range estimation algorithm the work proposed. Kalman filtering was applied in [108] with the measure-predict-update cycle applied on RSSI measurements to eliminate random noise and smoothen the measurements.

Although [68] gives an outline of existing filtering methods for RSSI in a general context comprising both range-estimation and tracking, quantitative results were not shown. The different techniques for preprocessing and filtering of RSSI for range-based estimation have therefore not been studied in sufficient detail to the best of our knowledge. We elaborate on select filtering methods later in this work.

Summary

This chapter highlighted related and background works in cooperative indoor localization. Localization algorithms, localization under incomplete information, localization under NLOS effects, RF communication and data preprocessing were reviewed in the light of some important existing works.

Chapter 3

Localization with MDS

"An algorithm must be seen to be believed."

Donald Knuth

MDS is a statistical method that transforms measurements of similarity (or dissimilarity) among pairs of objects into points in a low dimensional space where the distance between the objects are preserved [9]. MDS has been largely applied for the visualization of data in political science, sociology and psychology and has been alternatively referred to multidimensional similarity structure analysis [10] or smallest space analysis [37].

In the context of indoor localization, for environments where interaction between nodes are tightly coupled, it is often desirable to produce coherent location data that represents the state of all the objects in the environment at a glance. For such a cooperative localization task, MDS has proven itself a viable option. Since MDS-based localization utilizes pairwise distance measurements, the collection of these measurements is an important part of this localization scheme and the membership of nodes should be kept as flexible as possible to avoid estimation failure when any of the nodes suffer communication errors or goes offline.

This chapter introduces a formulation of MDS for localization with anchors initially derived in [30], which we extend for scenarios with missing tag interactions. Performance of the extended form over existing approaches is validated by simulations. As part of the measurement collection process, we briefly discuss a technique for managing node membership in the final part of the chapter.

3.1 Formulating Localization with MDS

Given measurements of distances among pairs of objects, localization with MDS places each object in a P-dimensional space (where P is usually 2 or 3) such that

the distance information in the estimated configuration matches the initial distance measurements as closely as possible.

In order to test the goodness of the configuration, MDS uses a cost function known as *Stress* σ defined on the computed configuration $\mathbf{X}$ as:

$$\sigma(\mathbf{X}) = \sum_{i<j\leq N} w_{ij}(\delta_{ij} - d_{ij}(\mathbf{X}))^2 \tag{3.1}$$

$$w_{ij} = \begin{cases} 1, & \text{if } \delta_{ij} \text{ is known} \\ 0, & \text{if } \delta_{ij} \text{ is missing} \end{cases} \tag{3.2}$$

where $d_{ij}(\mathbf{X})$ is the distance between nodes i and j defined for N nodes, δ_{ij} is the measured distance, and w_{ij} is the associated weight to distance measurement d_{ij} giving a measure of how accurate the distance is, when a measure of relative distance accuracies or importance is known. Other weighting structures beside the one in eq. (3.2) can be used, as long as $w_{ij} \geq 0$ [9]. Usually, $\mathbf{W}$ – the matrix of weights w_{ij} – is hollow, symmetric and non-negative.

3.1.1 Stress Majorization

One elegant method for solving MDS problems is *stress majorization*. To compute a configuration $\mathbf{X}$ that preserves the distance between nodes in the distance matrix, stress majorization proposes minimizing a convex function τ which bounds σ (the complicated function given by eq. (3.1)) from above and touches its surface at a point referred to as the supporting point. The minimization is done iteratively until eq. (3.3) is satisfied after which $\mathbf{X}^{(i)}$ i.e. the configuration calculated at the i-th iteration, converges to a configuration $\mathbf{X}$. This iterative procedure is referred to as Scaling by Majorizing a Complicated Function (SMACOF).

$$\sigma(\mathbf{X}^{(i-1)}) - \sigma(\mathbf{X}^{(i)}) < \epsilon \tag{3.3}$$

To arrive at a bounded complicated function, eq. (3.1) is first expanded as follows:

$$\begin{aligned} \sigma(\mathbf{X}) &= \sum_{i<j} w_{ij}\delta_{ij}^2 + \sum_{i<j} w_{ij} d_{ij}(\mathbf{X})^2 - 2 \cdot \sum\nolimits_{i<j} w_{ij}\delta_{ij} d_{ij}(\mathbf{X}) \\ &= \eta_\delta^2 + \eta(\mathbf{X})^2 - 2\rho(\mathbf{X}). \end{aligned} \tag{3.4}$$

From eq. (3.4), the first term η_δ^2 is constant, while the second term $\eta(\mathbf{X})^2$ is quadratic and therefore convex in $\mathbf{X}$. This second term is easily expressed in the form of the configuration of points $\mathbf{X}$ using the matrix trace operation tr as follows:

$$\begin{aligned} \eta(\mathbf{X})^2 &= \sum_{i<j} w_{ij} d_{ij}(\mathbf{X})^2 \\ &= \mathrm{tr}\mathbf{X}'\mathbf{V}\mathbf{X}. \end{aligned} \tag{3.5}$$

where the elements v_{ij} of the matrix $\mathbf{V}$ are defined as:

$$v_{ij} = \begin{cases} -w_{ij} & i \neq j \\ -\sum_{j=1, j\neq i}^{N} v_{ij} & i = j \end{cases} \tag{3.6}$$

The last term $-2\rho(\mathbf{X})$ is a weighted sum of distances $d_{ij}(\mathbf{X})$ since w_{ij} and δ_{ij} are constants and can be rewritten more clearly as:

$$-2\rho(\mathbf{X}) = -2 \cdot \sum\nolimits_{i<j} (w_{ij}\delta_{ij}) d_{ij}(\mathbf{X}). \tag{3.7}$$

The distance $d_{ij}(\mathbf{X})$ is upper-bounded by first applying the Cauchy-Schwarz inequality:

$$\begin{aligned} (\mathbf{x}_i - \mathbf{x}_j)'(\mathbf{z}_i - \mathbf{z}_j) &\leq \|\mathbf{x}_i - \mathbf{x}_j\| \cdot \|\mathbf{z}_i - \mathbf{z}_j\| \\ &\leq d_{ij}(\mathbf{X}) d_{ij}(\mathbf{Z}) \end{aligned} \tag{3.8}$$

where $\mathbf{x}_i$ and $\mathbf{x}_j$ are the i-th and j-th rows of the coordinate matrix $\mathbf{X}$ expressed as vectors. Rearranging eq. (3.8), we obtain a bound on $-d_{ij}(\mathbf{X})$:

$$-d_{ij}(\mathbf{X}) \leq -\frac{(\mathbf{x}_i - \mathbf{x}_j)'(\mathbf{z}_i - \mathbf{z}_j)}{d_{ij}(\mathbf{Z})}. \tag{3.9}$$

Substituting the result of eq. (3.9) into eq. (3.8), we obtain:

$$\begin{aligned} -2\rho(\mathbf{X}) &\leq -2 \cdot \sum\nolimits_{i<j} \frac{w_{ij}\delta_{ij}}{d_{ij}(\mathbf{Z})} (\mathbf{x}_i - \mathbf{x}_j)'(\mathbf{z}_i - \mathbf{z}_j) \\ &= -2\text{tr } \mathbf{X}'\mathbf{B}(\mathbf{Z})\mathbf{Z} \end{aligned} \tag{3.10}$$

so that ρ is now bounded by a function which is linear in $\mathbf{X}$. The matrix $\mathbf{B}(\mathbf{X})$ has elements b_{ij} defined by:

$$b_{ij} = \begin{cases} -\frac{w_{ij}\delta_{ij}}{d_{ij}(\mathbf{Z})} & d_{ij}(\mathbf{Z}) \neq 0, i \neq j \\ 0 & d_{ij}(\mathbf{Z}) = 0, i \neq j \\ -\sum_{j=1, j\neq i}^{N} b_{ij} & i = j \end{cases} \tag{3.11}$$

Finally, combining eq. (3.5) and eq. (3.10) and substituting into eq. (3.4), we derive:

$$\begin{aligned} \sigma(\mathbf{X}) &= \eta_\delta^2 + \text{tr } \mathbf{X}'\mathbf{V}\mathbf{X} - 2\text{tr } \mathbf{X}'\mathbf{B}(\mathbf{X})\mathbf{X} \\ &\leq \eta_\delta^2 + \text{tr } \mathbf{X}'\mathbf{V}\mathbf{X} - 2\text{tr } \mathbf{X}'\mathbf{B}(\mathbf{Z})\mathbf{Z} = \tau(\mathbf{X}, \mathbf{Z}) \end{aligned} \tag{3.12}$$

The minimum of the majorizing function $\tau(\mathbf{X}, \mathbf{Z})$ can be derived analytically by setting the derivative of $\tau(\mathbf{X}, \mathbf{Z})$ to zero:

$$\nabla\tau(\mathbf{X}, \mathbf{Z}) = 2\mathbf{V}\mathbf{X} - 2\mathbf{B}(\mathbf{Z})\mathbf{Z} = 0$$

yielding a solution which has been shown to decrease the stress σ monotonically [19, 59]:

$$\begin{aligned}\hat{\mathbf{X}} &= \min_{X} \tau(\mathbf{X}, \mathbf{Z}) \\ &= \mathbf{V}^{+}\mathbf{B}(\mathbf{Z})\mathbf{Z}.\end{aligned} \tag{3.13}$$

Equation (3.13) is called the *Guttman transform*. The Moore-Penrose pseudoinverse $\mathbf{V}^{+}$ is used since $\mathbf{V}$ is not full-rank. The iterative solution can be rewritten as an update form of eq. (3.13), where $\mathbf{Z}$ is the value of $\mathbf{X}$ for the current iteration:

$$\mathbf{X}^{(k+1)} = \mathbf{V}^{+}\mathbf{B}(\mathbf{X}^{(k)})\mathbf{X}^{(k)}. \tag{3.14}$$

Equation (3.14) is usually initialized with a random configuration of points $\mathbf{X}^{(0)}$ and generates a suitable configuration of points whose euclidean distances matches closely the matrix of distance measurements δ when eq. (3.3) is satisfied. This final configuration of points is not unique for each δ. Unique solutions can be obtained by the adding position of fixed nodes to the initial random configuration as discussed in section 3.1.2.

3.1.2 Stress Majorization with Fixed Anchor Positions

In section 3.1.1, the tag locations were derived by minimizing the majorizing function τ on the partial configuration of tags $\mathbf{X}_t \subset \mathbf{X}$. With known exact values of anchor positions $\mathbf{X}_a \subset \mathbf{X}$, the unknown tag positions $\mathbf{X}_t$ where derived with respect to $\mathbf{X}_a$ by eliminating the need for the usual roto-translation in previous worksand improving the accuracy of tag positions. To find the value of $\mathbf{X}_t$ that minimizes τ, we take the partial derivative of τ w.r.t. $\mathbf{X}_t$:

$$\frac{\partial \tau(\mathbf{X}, \mathbf{Z})}{\partial \mathbf{X}_t} = \frac{\partial \eta_\delta^2}{\partial \mathbf{X}_t} + \frac{\partial(\text{tr } \mathbf{X}'\mathbf{V}\mathbf{X})}{\partial \mathbf{X}_t} - 2\frac{\partial\,(\text{tr } \mathbf{X}'\mathbf{B}(\mathbf{Z})\mathbf{Z})}{\partial \mathbf{X}_t} \tag{3.15}$$

The first term in eq. (3.15) is zero, while the other terms are more easily solvable if the coordinate matrix $\mathbf{X}$ is partitioned into matrices $\mathbf{X}_t$ and $\mathbf{X}_a$:

$$\mathbf{X} = \begin{bmatrix}\mathbf{X}_t \\ \mathbf{X}_a\end{bmatrix}.$$

The matrices $\mathbf{B}$ and $\mathbf{V}$ are also partitioned into components that correspond to the $\mathbf{X}$ matrix partitions, which are defined as follows:

$$\mathbf{V} = \begin{bmatrix}\mathbf{V}_{11} & \mathbf{V}_{12} \\ \mathbf{V}'_{12} & \mathbf{V}_{22}\end{bmatrix},\ \mathbf{B}(\mathbf{Z}) = \begin{bmatrix}\mathbf{B}_{11} & \mathbf{B}_{12} \\ \mathbf{B}'_{12} & \mathbf{B}_{22}\end{bmatrix} \tag{3.16}$$

where $\mathbf{V}_{11}, \mathbf{B}_{11} \in \mathbb{R}^{m\times m}$, $\mathbf{V}_{12}, \mathbf{B}_{12} \in \mathbb{R}^{m\times n}$, and $\mathbf{V}_{22}, \mathbf{B}_{22} \in \mathbb{R}^{n\times n}$. The dimension values m and n are the number of tags and anchors respectively.

To take the derivative of the trace of the matrix products we transform to a scalar form using index notation so that the second term in eq. (3.12) can be rewritten in the form of column vectors $\mathbf{x}_i$ as:

$$\begin{aligned} \text{tr } \mathbf{X}'\mathbf{V}\mathbf{X} &= \sum_{i=1}^{P} \mathbf{x}'_{(i)}\mathbf{V}\mathbf{x}_{(i)} \\ &= \sum_{i=1}^{P} \left(\mathbf{x}'_{t(i)}\mathbf{V}_{11}\mathbf{x}_{t(i)} + 2\mathbf{x}'_{t(i)}\mathbf{V}_{12}\mathbf{x}_{a(i)} + \mathbf{x}'_{a(i)}\mathbf{V}_{22}\mathbf{x}_{a(i)} \right), \end{aligned} \tag{3.17}$$

and the second term in eq. (3.15) can now be written as:

$$\frac{\partial(\text{tr } \mathbf{X}'\mathbf{V}\mathbf{X})}{\partial \mathbf{X}_t} = 2(\mathbf{V}_{11}\mathbf{X}_t + \mathbf{V}_{12}\mathbf{X}_a) \tag{3.18}$$

Similarly, the third term in eq. (3.12) can be expanded as:

$$\begin{aligned} \text{tr } \mathbf{X}'\mathbf{B}(\mathbf{Z})\mathbf{Z} &= \sum_{i=1}^{P} \mathbf{x}'_{(i)}\mathbf{B}(\mathbf{Z})\mathbf{z}_{(i)} \\ &= \sum_{i=1}^{P} \left(\mathbf{x}'_{t(i)}\mathbf{B}_{11}\mathbf{z}_{t(i)} + 2\mathbf{x}'_{t(i)}\mathbf{B}_{12}\mathbf{z}_{a(i)} + \mathbf{x}'_{a(i)}\mathbf{B}_{22}\mathbf{z}_{a(i)} \right), \end{aligned} \tag{3.19}$$

and its derivative in eq. (3.15) is now also easily solvable:

$$\frac{\partial(\text{tr } \mathbf{X}'\mathbf{B}(\mathbf{Z})\mathbf{Z})}{\partial \mathbf{X}_t} = \mathbf{B}_{11}\mathbf{Z}_t + \mathbf{B}_{12}\mathbf{Z}_a \tag{3.20}$$

Substituting the terms in eq. (3.18) and eq. (3.20) into eq. (3.15), and equating to zero to find the minimum of τ, we have:

$$\frac{\partial \tau(\mathbf{X}, \mathbf{Z})}{\partial \mathbf{X}_t} = 2(\mathbf{V}_{11}\mathbf{X}_t + \mathbf{V}_{12}\mathbf{X}_a - \mathbf{B}_{11}\mathbf{Z}_t - \mathbf{B}_{12}\mathbf{Z}_a) = 0 \tag{3.21}$$

The partial support $\mathbf{Z}_a \in \mathbf{Z}$, which is a point on τ, has a known solution $\mathbf{X}_a$ in σ, so that generally $\mathbf{Z}_a \approx \mathbf{X}_a$ and $\mathbf{Z}_a \approx \mathbf{X}_a$ if σ is convex, i.e. $\sigma = \tau$. Substituting $\mathbf{Z}_a$ as $\mathbf{X}_a$ and solving for $\mathbf{X}_t$:

$$\mathbf{X}_t = \mathbf{V}_{11}^{-1}\left(\mathbf{B}_{11}\mathbf{Z}_t + (\mathbf{B}_{12} - \mathbf{V}_{12})\mathbf{X}_a\right) \tag{3.22}$$

Finally, eq. (3.22) can be rewritten in an iterative form as:

$$\mathbf{X}_t^{(k+1)} = \mathbf{V}_{11}^{-1}\left(\mathbf{B}_{11}\mathbf{X}_t^{(k)} + (\mathbf{B}_{12} - \mathbf{V}_{12})\mathbf{X}_a\right) \tag{3.23}$$

where the initial guess $\mathbf{X}_t^{(0)}$ is a coordinate matrix with random values.

3.2 Handling Missing Tag Interactions

From eq. (3.23), we proceed to formulate an extended Anchored MDS (MDS-A) approach for the case with missing tag-to-tag distances. Given a distance matrix $\mathbf{D}$ (eq. (3.24)) for a setup with m tags and n anchors (so that $m+n=N$), and missing within-sets (between nodes of the same type) distances for tags, the distance matrix is again partitioned so that eq. (3.23) becomes applicable:

$$\mathbf{D} = \begin{bmatrix} \mathbf{\Lambda} & \mathbf{D}_{12} \\ \mathbf{D}_{12}^T & \mathbf{D}_{22} \end{bmatrix} \tag{3.24}$$

where $\mathbf{\Lambda}$ is the submatrix of missing tag-to-tag proximities, $\mathbf{D}_{12}, \mathbf{D}_{21}$ are anchor-to-tag distances and $\mathbf{D}_{22}$ are anchor-to-anchor distances.

For a sufficiently large amount of iterations, as $k \to \infty$, we know that the support point of the majorizing convex function is a stationary point, so that $\mathbf{X}^{(k+1)} \approx \mathbf{X}^{(k)}$. One consequence of the convergence of eq. (3.14) is that $\mathbf{B}(\mathbf{X}^{(k)})$ tends to $\mathbf{V}$:

$$\mathbf{V} \approx \lim_{k\to\infty} \mathbf{B}(\mathbf{X}^{(k)}) \tag{3.25}$$

The limit in eq. (3.25) is an equality when there is zero noise in the distance measurements. To extend eq. (3.25) for the MDS-A solution described in eq. (3.23), we can have $\mathbf{X}_t^{(k+1)} \approx \mathbf{X}_t^{(k)}$, by setting $(\mathbf{B}_{12} - \mathbf{V}_{12})\mathbf{X}_a$ to 0 leading to eq. (3.26).

$$\mathbf{V}_{11} \approx \lim_{k\to\infty} \mathbf{B}_{11}(\mathbf{X}^{(k)}) \tag{3.26}$$

Since the tag within-sets distances are unknown, we can compute each tag location independent of the others by making $\mathbf{B}_{11}$ a diagonal matrix, with its diagonal elements being the sum of elements from the neighbouring $\mathbf{B}_{12}$ partition:

$$\mathbf{B_{11}} = \begin{bmatrix} -\sum_{j\neq 1}^{n} b_{1j} & 0 & \cdots & 0 \\ 0 & -\sum_{j\neq 2}^{n} b_{2j} & \cdots & 0 \\ \vdots & \vdots & \ddots & \\ 0 & 0 & & -\sum_{j\neq m}^{n} b_{mj} \end{bmatrix}$$

To avoid making assumptions about the tag within-sets distances $\mathbf{\Lambda}$ as with MDS-RFID, the off-diagonal elements of $\mathbf{B}$ can only be zero if their corresponding weights in $\mathbf{W}$ are 0 in conformance with eq. (3.11).

By setting the missing tag within-sets weights to 0, the weight matrix $\mathbf{W}$ is now partitioned as in eq. (3.27) where $\mathbf{1}\mathbf{1}_{m,n}$ is a matrix of ones with shape $m \times n$.

$$\mathbf{W} = \begin{bmatrix} \mathbf{0} & \mathbf{W}_{12} \\ \mathbf{W}_{12}^T & \mathbf{W}_{22} \end{bmatrix} = \begin{bmatrix} \mathbf{0}_{m,m} & \mathbf{1}\mathbf{1}_{m,n} \\ \mathbf{1}\mathbf{1}_{m,n}^T & \mathbf{1}\mathbf{1}_{n,n} \end{bmatrix} \tag{3.27}$$

The matrix $\mathbf{V}$ (eq. (3.28)) can now be computed in partitions from $\mathbf{W}$ using eq. (3.6).

$$\mathbf{V} = \begin{bmatrix} n\mathbf{I} & -\mathbf{1}\mathbf{1}_{m,n} \\ -\mathbf{1}\mathbf{1}_{m,n}^T & (m+n)\mathbf{I} - \mathbf{1}\mathbf{1}_{n,n} \end{bmatrix} \tag{3.28}$$

This way, $\mathbf{V}_{11}$ now satisfies eq. (3.26) and its inverse can be written as in eq. (3.29) and $\mathbf{V}_{12}$ as in eq. (3.30).

$$\mathbf{V}_{11}^{-1} = \mathbf{I}/n \tag{3.29}$$

$$\mathbf{V}_{12} = -\mathbf{1}\mathbf{1}_{m,n} \tag{3.30}$$

Matrix $\mathbf{V}_{12}$ also satisfies the earlier assumption that $(\mathbf{B}_{12} - \mathbf{V}_{12})\mathbf{X}_a = 0$ at some sufficiently large iteration number k where $\mathbf{B_{12}} = -\mathbf{1}\mathbf{1}_{m,n}$, since $\delta_{ij} = d_{ij}(\mathbf{X})$ for between-sets distances when there is no noise in the measurements.

The $\mathbf{B}$ matrix (eq. (3.31)) is similarly partitioned as with $\mathbf{W}$ and $\mathbf{V}$, where each partition of $\mathbf{B}$ is computed as in eq. (3.11).

$$\mathbf{B} = \begin{bmatrix} \mathbf{B}_{11} & \mathbf{B}_{12} \\ \mathbf{B}_{12}^T & \mathbf{B}_{22} \end{bmatrix} \tag{3.31}$$

Substituting eq. (3.29) and eq. (3.30) into eq. (3.23) we arrive at a simplified update procedure for $\mathbf{X}_t$ that does not consider the interaction between tags:

$$\mathbf{X}_t^{(k+1)} = \frac{\mathbf{B}_{11}\mathbf{X}_t^{(k)} + (\mathbf{B}_{12} + \mathbf{1}\mathbf{1}_{m,n})\mathbf{X}_a}{n}. \tag{3.32}$$

The update in eq. (3.32) is done with the SMACOF iterative process until the convergence condition in eq. (3.3) is satisfied. The final configuration $\mathbf{X}$ can now be constructed trivially:

$$\mathbf{X} = \begin{bmatrix} \hat{\mathbf{X}}_t \\ \mathbf{X}_a \end{bmatrix}.$$

When tag interactions are missing, the anchor-tag between-sets distances can give a full representation of the distance matrix requiring $\mathrm{O}(m \times n)$ storage; anchor within-sets are not required since anchor locations are fixed and tag within-sets distance are missing. Since implementations of the SMACOF algorithm do not take non-symmetrical matrices as input, placeholder values should be used in place of the missing tag within-sets distances.

An implementation of our work in Python containing these details can be found at [53], which also includes the related experiments in section 3.2.1.

3.2.1 Experimental Results

In this section, we describe experiments comparing our results for handling missing distances described in section 3.2 with an existing technique that estimates missing inter-tag distances, MDS-RFID [88], and the classical MDS.

In a simulated deployment region of $30m \times 20m$ area, the number of tags, anchors and measurement noise were varied in different experiments. Noise is only added to the between-sets distances since anchor positions are known and their within-sets distances are not part of the measurements. The noise in the distances is modeled as Gaussian for simplicity, as:

$$\hat{d_{ij}} = d_{ij}(\mathbf{X}) + \mathcal{N}(0,\, \sigma^2).$$

Figures 3.1a and 3.1b show sample runs of MDS-RFID and our specialized MDS-A algorithms using 4 anchors, 7 tags and $\sigma = 1$. Results for classical MDS are not shown since an extensive study has already been demonstrated in [30].

We note here that the MDS-RFID as discussed in [88] uses eigenvalue decomposition (EVD) to solve the MDS problem. However, in our experiments, it has been used with the SMACOF algorithm which allows to set the weights of the estimated missing distances to a value that gives the lowest Root Mean Squared Error (RMSE). This weight $w_{t(ij)}$ has been found to be 0.7 by heuristics for this particular set of experiments. The RMSE in each experiment that evaluates accuracy of the computed configuration with respect to the original configuration is given by eq. (3.33).

$$RMSE = \sqrt{\frac{1}{N}\sum_{i=1}^{N} \|x_i - \hat{x}_i\|^2} \tag{3.33}$$

In the following paragraphs, we describe the various experiments and their results. Each of them have been repeated with 100 trials, taking initial guess $\mathbf{X}_t^{(0)}$ of the SMACOF algorithm for all the trials randomly.

The first experiment checks the effects of noise and number of tags (i.e., the proportion of missing data) on the RMSE of modified MDS-A. The results were compared with those of full connectivity, where tag within-sets data is available. In the first case shown in Figure 3.2a, the number of anchors was kept constant at 4, while σ was varied. In the second case shown in Figure 3.2b, σ was kept constant while the number of tags (amount of missing data) was varied. The disparity in both methods is not unexpected and suggests that discarding some measurements such as non line-of-sight distances would further degrade the performance, motivating the need to develop a more robust solution (addressed in this document in chapter 4).

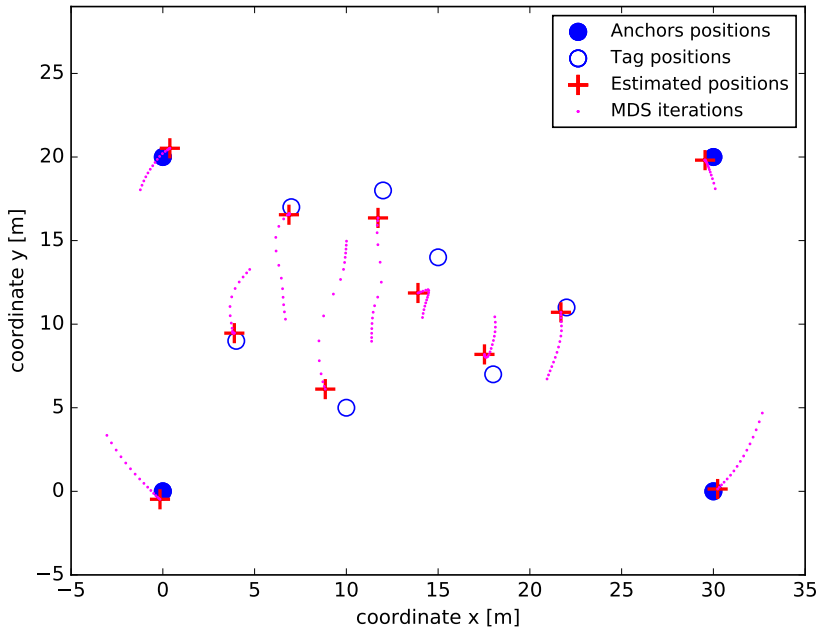

(a) MDS-RFID under missing tag-to-tag distances and $\mathcal{N}(0, 1)$ measurement noise.

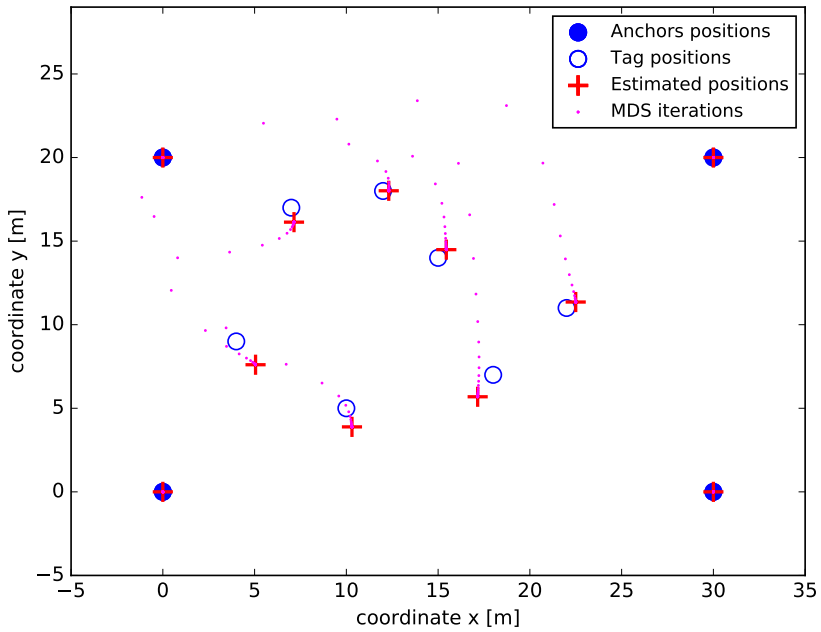

(b) MDS-A (extended form) under missing tag-to-tag distances and $\mathcal{N}(0, 1)$ measurement noise.

Figure 3.1: Errors in estimated positions are at least 30% lower in (b) than in (a).

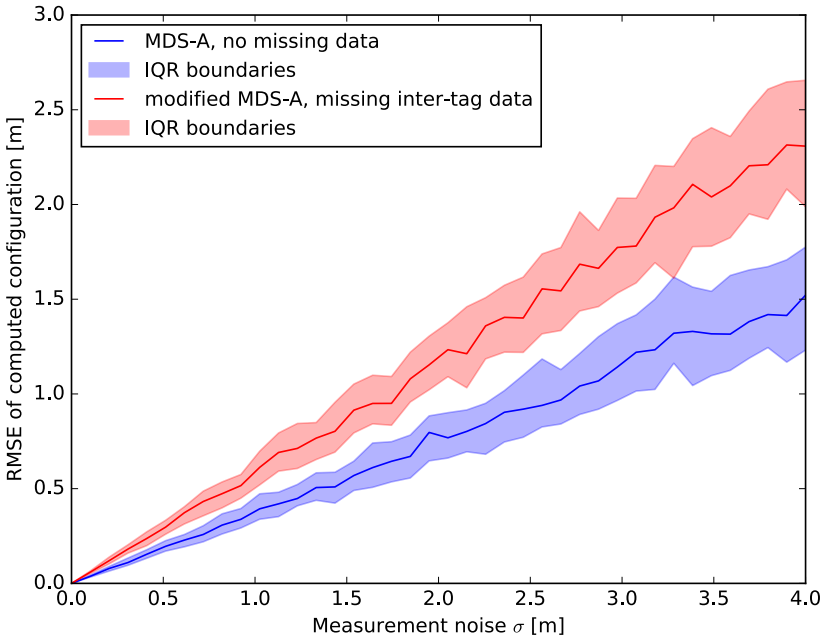

(a)

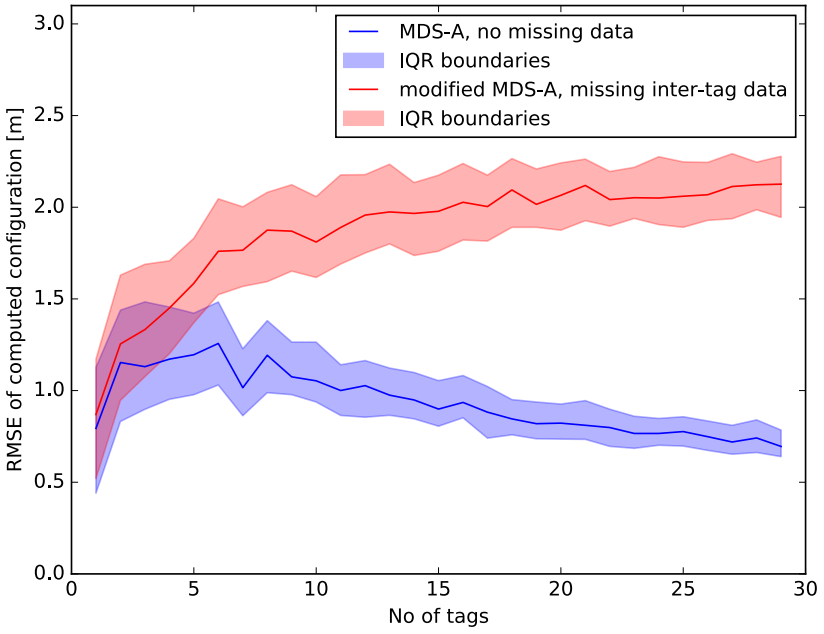

(b)

Figure 3.2: Median and IQR of RMSE with MDS-A and modified MDS-A (with tag-to-tag distances removed). 3.2a: σ is varied from 0 to 4 in steps of 0.1 while number of tags is 10; 3.2b: number of tags is varied from 1 to 30 while $\sigma = 3$.

Figure 3.3a shows the median and interquartile range (IQR) of the RMSE for classical MDS, MDS-RFID, and the specialized MDS-A when the value of σ is varied in steps of 0.1 from 0 to 4. The RMSE increases monotonically with the error for all three methods. Although MDS-RFID has the highest RMSE at $\sigma = 0$, it is much more robust to increasing error than classical MDS, and the IQR of the RMSE is more constrained. Overall, the specialized MDS-A form performs better than the other methods.

Results for the experiment involving a variation of the number of anchors is shown in Figure 3.3b. The σ value set at 3 allows to properly study the influence of the number of anchors for each of the methods in high error situations. The MDS-RFID algorithm performs better than the classical MDS and slightly better than modified MDS-A when the number of anchors is set to 3. This can be attributed to the optimal weights used for the recovered distances, which as stated earlier was found by heuristics. If the weight values were 1, i.e. giving both existing and recovered distances same weight, the specialized MDS-A form will outperform MDS-RFID. Moreover, as the number of anchors increases, our approach takes advantage of the available anchor information, so that its median RMSE is less than those of MDS-RFID and classical MDS.

3.3 Dynamic Node Membership

The matrix of pairwise distances is constructed from distance measurements between nodes for all active nodes in the deployment region by stacking each node's set of pairwise distances with every node along rows and columns. New nodes can be added dynamically by stacking their pairwise distance information from every anchor to the rows and columns of the distance matrix. An illustration of this operation is depicted in fig. 3.4, where the number of tags m goes from 1 to 2.

As the new node, labeled 5, comes on, the hardware stack automatically adds the node to the list of tracked nodes and its distance information is forwarded to the software stack alongside those of the existing nodes. In the software stack, the new member's vector of pairwise distances are transposed, and the original and transposed forms are used for stacking. From fig. 3.4, we notice that the distance between tag 4 and 5, $d_{45} = d_{54}$, is recorded as 0 since tags do not interact with each other. When the stacking is performed, a final 0 is automatically added to the last diagonal position to complete the square matrix.

On a similar note, when a mobile node goes offline, its distance information gets deleted from the rows and columns of the matrix so that the size of the distance

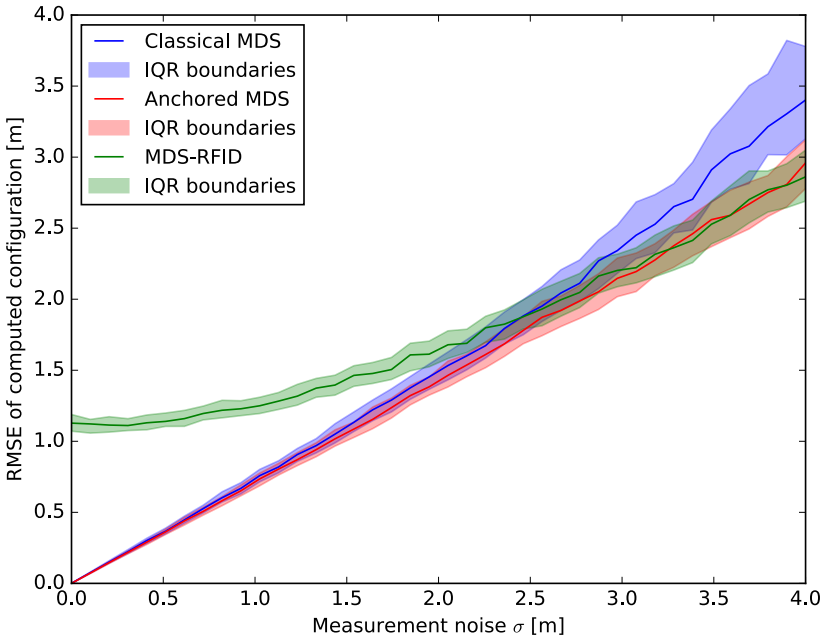

(a)

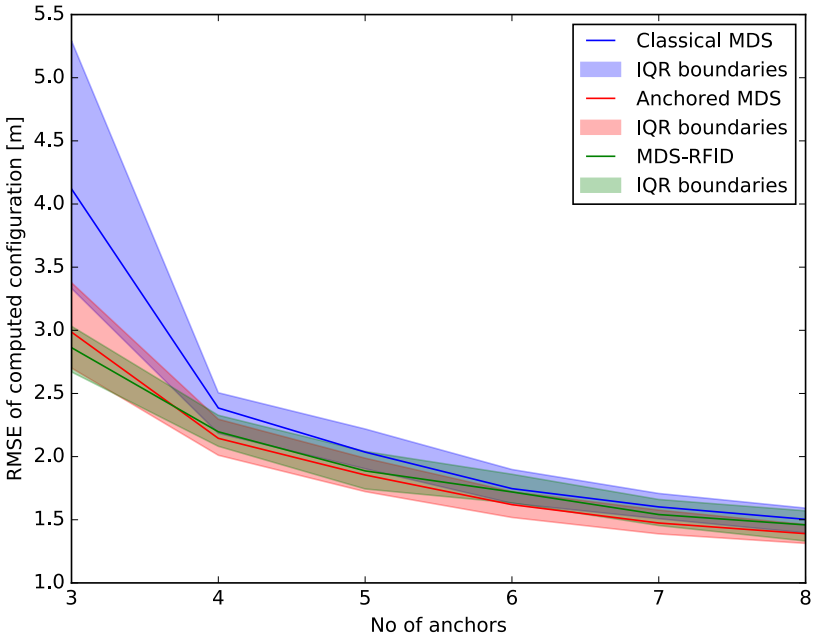

(b)

Figure 3.3: Median and IQR of RMSE for MDS-RFID, classical MDS and modified MDS-A. In 3.3a, σ is varied from 0 to 4 in steps of 0.1 while number of tags is 30, and in 3.3b, number of anchors is varied from 3 to 8 while $\sigma = 3$.

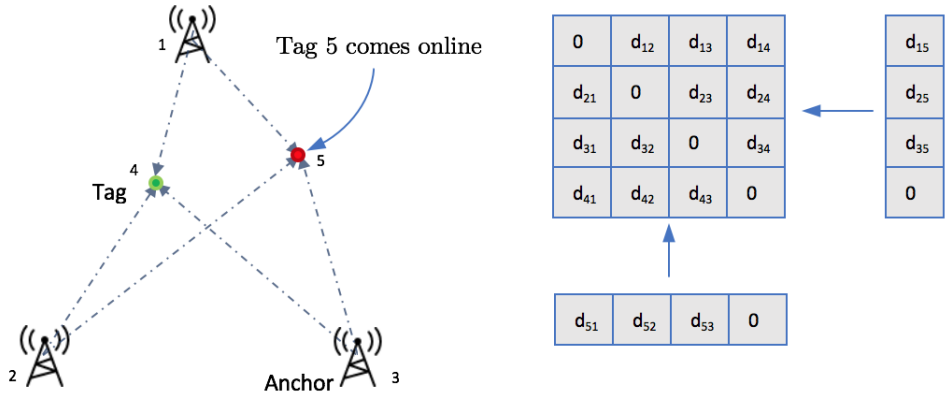

Figure 3.4: Pairwise distance information of new node is padded to distance matrix as the node comes online.

matrix shrinks and the value of m is update with $m - 1$ after the deletion.

Summary

In this chapter, we introduced MDS in the context of localization. A specialized formulation of MDS-A was formulated, which has shown to provide better results than existing techniques for handling missing data. We show that by decoupling the interaction between tags, tag locations can be inferred directly from the available anchors when tag-to-tag distances are missing. This undermines (but does not eliminate) the effect of the missing data without making assumptions about the relative distances between tags. Experiments demonstrate the performance of this specialized MDS-A over MDS-RFID and classical MDS.

In the last part of the chapter, we introduced a simple technique for managing node memberships such that node additions and removals do not interfere with the localization algorithm.

Chapter 4

Localization in NLOS Environments

"If we knew what it was we were doing, it would not be called research, would it?"

Albert Einstein

In this chapter, indoor localization under so-called *nonline-of-sight* (NLOS) conditions is considered. Under range-based radio positioning, the occurrence of multipath and attenuation effects caused by obstacles, occlusions or interference in the deployment region of radio positioning nodes contribute negatively to the performance of indoor positioning algorithms. A physical object lying between transmitter and receiver such that there is no clear visual line of sight between both will cause the transmitted signal 1) to be attenuated or diffracted if the obstacle is not completely blocking or 2) to travel a different path leading to anomalies at the receiving end. This would often cause the RSS to be weakened or cause the ToF to take longer, making the estimated distance to be longer than the actual length; these anomalies are classified in this work as *nonline-of-sight (NLOS) effects*. Figure 4.1 gives a pictorial description of a signal not having clear line-of-sight between anchor and tag.

The MDS with anchors approach discussed in chapter 3 is adapted for the mitigation of NLOS bias that is presented later in this chapter. Application scenarios for MDS-A in NLOS environments where inter-tag interactions are missing are not uncommon. One advantage of removing inter-tag interaction is, firstly, reduced architecture complexity and time required to collect all the required distance measurements in order to build a matrix (the matrix is sparse) and secondly, the elimination of further NLOS biases and noise that may be present in the pairwise distances between tags. The latter has shown to be vital for the performance of our

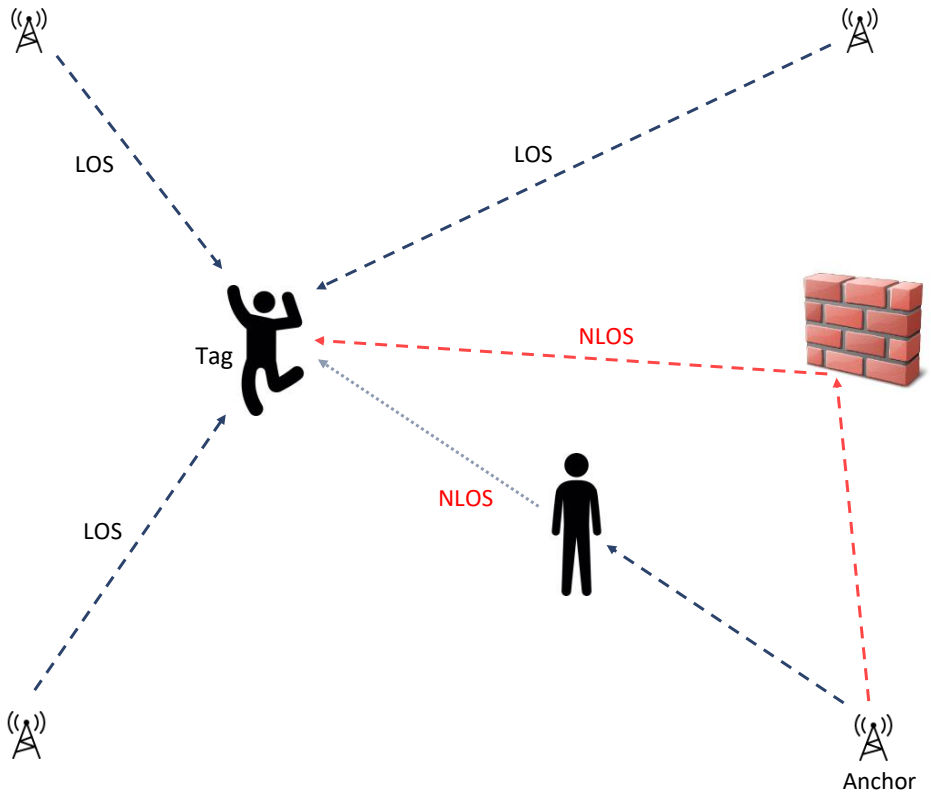

Figure 4.1: NLOS effects from physical object lying between anchor and object on which tag is placed.

proposed NLOS mitigation scheme since tag positions only receive support from anchor-tag distances in the localization algorithm. Examples of such deployments can be found in:

1. localization schemes that use single/round-trip ToF between fixed and mobile nodes,

2. localization schemes where mobile nodes read RSSI for signal transmissions from fixed nodes or the other way around.

The mobility of nodes contributes to vulnerability to NLOS effects since objects to which the nodes are attached can obstruct one another and proximity to walls and large metallic objects increases signal reflection which in turn distorts the signal.

4.1 Reasoning and Problem Formulation

In this section, we formulate an NLOS mitigation technique under the MDS scheme. In fig. 4.2a, we show the received signal strengths from 4 nanoLoc [1] anchors measured from a stationary nanoLoc tag. In the setup, an object is moving around the tag at a non-constant speed and we notice how there are successive drops in signal strength from each anchor while there is an obstruction between itself and the stationary tag by the moving object. Even after the signals have been filtered, the dip values present problems as the computed distances appear larger for the duration of the occlusion. The lengthening of these computed distances can be observed in fig. 4.2b. Using these distances directly in a cooperative localization algorithm will lead to estimation errors in the form of sporadic jumps in tag positions. The task therefore is to estimate the amount of bias and noise in each of the distances.

For a matrix of NLOS and noise free pairwise distances, tag positions can be computed from those of anchors, and the anchor positions can be recomputed exactly from those of tags by swapping anchors with tags under the specialized MDS-A formulation. This symmetry in anchor-tag and tag-anchor estimation applies for node deployments with at least 3 tags and 3 anchors, and a matrix of distance measurements free of NLOS bias and measurement noise. In real life applications, this is hardly the case, as distances are almost never accurate. Moreover, since the aforementioned symmetry is lost, tag positions estimated from the skewed matrix do not represent the exact tag positions. We provide an estimate on the goodness of this skewed matrix by recomputing anchor positions from the earlier computed tag positions, and taking the error with respect to the known anchor positions. The error in the tentative anchor positions will be proportional to the amount of noise and NLOS bias in the matrix of distance measurements. We derive this error analytically and we formulate a constrained optimization problem to find bias values that yield the least error on tentative anchor positions. Since the tag within-sets distances are not available, the support for computation of tentative anchor positions is provided only by anchor-tag between-sets distances, therefore making the error a better reflection of between-sets NLOS biases and noise.

We verify the accuracy improvements of the proposed approach by experiments which indicate significant reductions in positioning RMSE by up to 28% for a setup of 4 anchors and 3 tags. Simulations are used to further demonstrate accuracy improvements for deployments involving an area with larger dimensions, and higher number of anchors and tags.

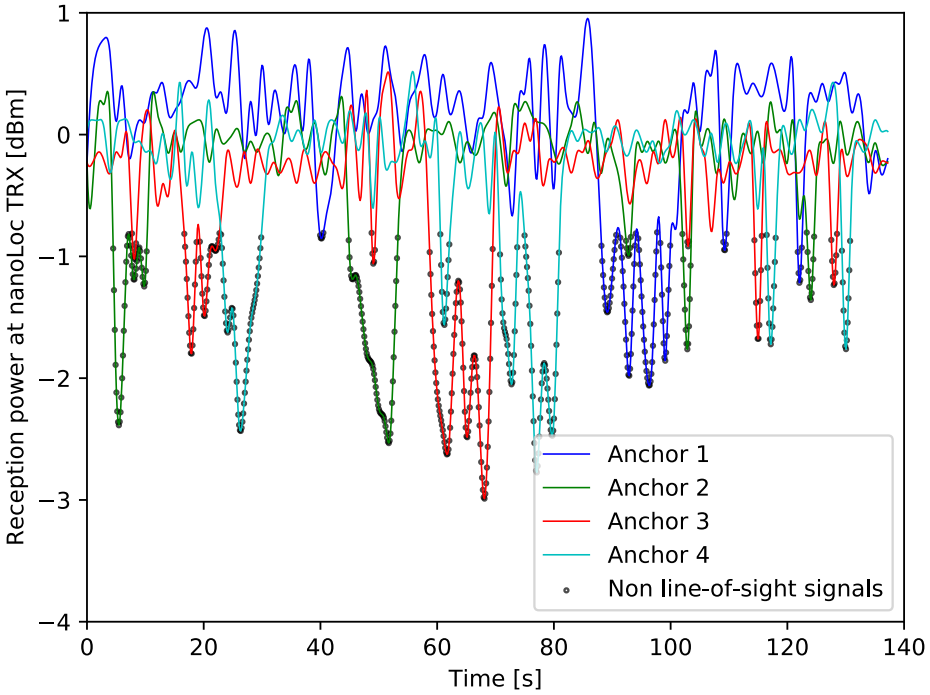

(a) Reception power measured from a stationary tag with an obstacle moving around it.

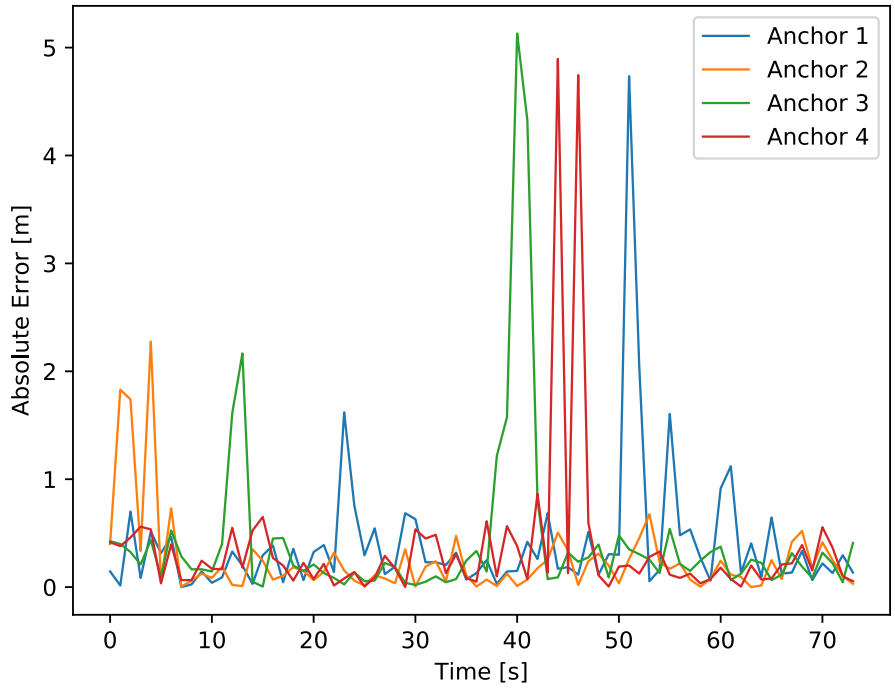

(b) Changes in distance measurements as seen from stationary tag with obstacle moving around it.

Figure 4.2: Effects of NLOS effects on RSS and distance measurements.

4.2 Cooperative Mitigation of NLOS Effects

As stated earlier, there exists an intrinsic symmetry in a matrix of LOS measurements of pairwise distances which allows to compute tag locations from anchor locations and then recompute exactly the same anchor positions from the earlier computed tag positions. Under NLOS conditions, there is no such symmetry; anchor positions can not be reproduced exactly from those of tags. In this section, we introduce mathematically our heuristic for the removal of NLOS in a matrix of pairwise distances. This heuristic is based on the knowledge of the aforementioned symmetric property of ideal distance matrices. In the presence of NLOS effects, the symmetry of the pairwise distance matrix is lost. However, the ensuing asymmetry allows to mitigate NLOS effects by minimizing the error on the recomputation of anchors.

In fig. 4.3, we show how the errors on the recomputation of anchor positions grows monotonically with increasing NLOS and measurement noise. The data for the plots was generated from simulations where NLOS effects and measurement noise are added to a distance matrix using the ToF error model described in [3] and tag positions are computed relative to anchor positions using the skewed distance matrix. The NLOS effects and noise were amplified using multiplicative factors, with a factor of zero indicating zero NLOS effects and noise. At each simulation, we take the sum of the errors on the tag positions and sum of the errors on the recomputation of anchors, using the earlier computed tags as anchors. The median values and IQR values for both error sums are plotted. The plots indicate that tag position errors are lower bounded by the anchor position errors, so that all of the NLOS effects and measurement noise are not completely traceable from anchor recomputation errors. This confirms that complete removal of NLOS effects and measurement noise is not possible, generally and under our proposed scheme in particular. We observe that there are no errors on anchor recomputation at zero NLOS and noise.

The tentative anchors positions $\tilde{\boldsymbol{X}}_a$ are recomputed by swapping anchors with tags in eq. (3.23), so that anchors are now recomputed from tag positions $\boldsymbol{X}_t$ using the anchor-tag between-sets distances as support. This yields a new equation of the following form:

$$\tilde{\boldsymbol{X}}_a = \frac{\boldsymbol{B}_{22}\boldsymbol{Z}_a + (\boldsymbol{B}_{21} + \mathbf{1}\mathbf{1}_{n,m})\boldsymbol{X}_t}{m} \tag{4.1}$$

From eq. (4.1), anchors positions are directly computable from those of tags if the number of tags $m \geq 3$, where 3 is the minimum number of fixed nodes sufficient for the computation of unique anchor positions. We present a supplementary approach

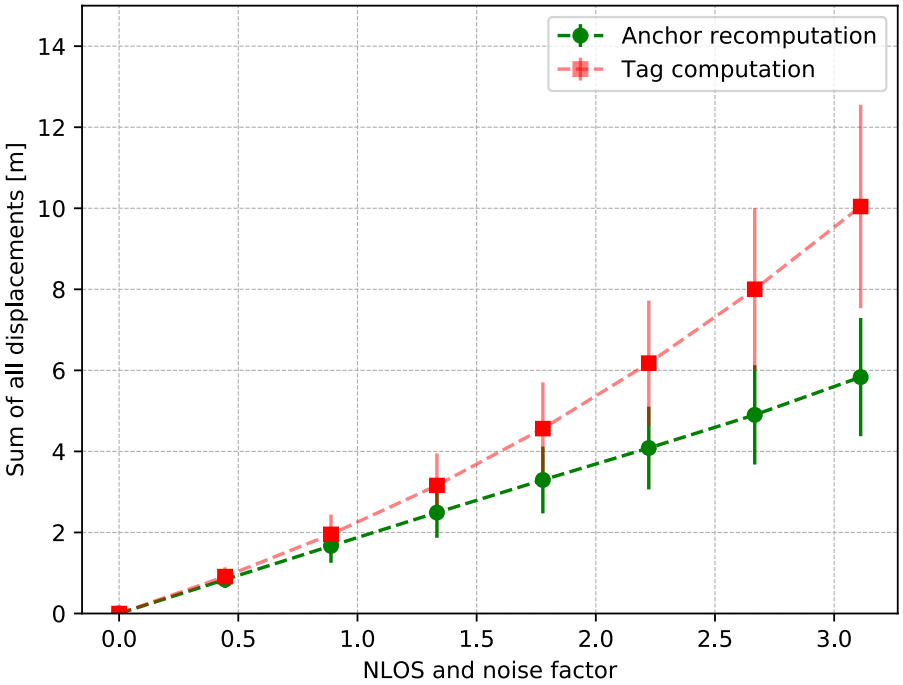

Figure 4.3: Correlation between position errors for tags and recomputed anchors.

in section 4.2.2 for special cases where the number of tags $m = 1$ and $m = 2$.

The error in the computation of the tentative anchor positions is the sum of the displacements between each recomputed position in the tentative anchor configuration $\tilde{\boldsymbol{X}}_a$ and its corresponding exact position in the known anchor configuration $\boldsymbol{X}_a$. This error e_a is expressed mathematically as:

$$e_a = \sum_{i=1}^{n} \|\tilde{\boldsymbol{x}}_{a(i)} - \boldsymbol{x}_{a(i)}\| \tag{4.2}$$

where $\tilde{\boldsymbol{x}}_{a(i)}$ and $\boldsymbol{x}_{a(i)}$ are the tentative and known positions of the i^{th} anchor respectively.

Since $\tilde{\boldsymbol{X}}_a$ is computed from a non-ideal matrix of distance measurements containing some unknown NLOS bias and measurement noise, then the equation for $\tilde{\boldsymbol{X}}_a$ can be rewritten as:

$$\tilde{\boldsymbol{X}}_a = \texttt{MDS}(\boldsymbol{X}_t,\ \boldsymbol{\delta} + \boldsymbol{b}). \tag{4.3}$$

where `MDS` indicates the MDS algorithm as a callable procedure that takes parameters $\boldsymbol{X}_t$, $\boldsymbol{\delta}$, $\boldsymbol{b}$ and returns a configuration of positions. We make no attempt to distinguish

NLOS effects from measurement noise, so that both are estimated jointly and cumulated in the matrix $\boldsymbol{b}$. Henceforth, we will refer to both NLOS bias and measurement noise as simply NLOS bias.

Equation (4.3) allows to also rewrite the error e_a as function of NLOS bias in a similar form:

$$e_a = \sum_{i=1}^{n} \|\texttt{MDS}(\boldsymbol{X}_t,\ \boldsymbol{b})_{(i)} - \boldsymbol{x}_{a(i)}\| \tag{4.4}$$

where the matrix of measured distances $\boldsymbol{\delta}$ has been dropped since its elements are constant.

The optimization problem for finding tag positions and NLOS bias values that minimize error e_a is now written as:

$$\hat{\boldsymbol{\theta}}_t = \min_{\boldsymbol{\theta}}\ e_a(\boldsymbol{X}_t,\ \boldsymbol{b}), \boldsymbol{\theta} = [\boldsymbol{X}_t\ \boldsymbol{b}]^T \tag{4.5}$$

The tag positions $\boldsymbol{X}_t$ are unconstrained since they are explicitly computed by eq. (3.32). However, the cumulated NLOS bias $b_{ij} \in \boldsymbol{b}$ are constrained so that their corresponding values for any of the distances are finite and positive (or zero). This condition can be formally expressed as:

$$b^L \leq b_{ij} \leq b^U, \quad \forall b_{ij} \in \boldsymbol{b}_\theta \tag{4.6a}$$

$$b_{ij} = 0, \quad \forall b_{ij} \notin \boldsymbol{b}_\theta \tag{4.6b}$$

where $\boldsymbol{b}_\theta \subset \boldsymbol{b}$ is the set of all anchor-tag between-sets biases. The lower bound b^L can be set as $b^L = 0$ for ideal distances while the upper bound b^U can be based on information regarding the geometrical layout of the deployment region, as proposed in [102]. The values for anchor within-sets NLOS biases are set to 0 since all anchor positions are known and their pairwise distances are ideal while those for tag within-sets are equally set to 0 since within-sets distances for tags are not available.

4.2.1 Deployments with at least 3 tags

When the number of tags is at least 3, i.e., $m > 3$, the tentative anchor positions can be computed by swapping anchors with tags described in eq. (4.1). The error function e_a is nonlinear with respect to $\boldsymbol{b}$ (the partial $\boldsymbol{B}$ matrices $\boldsymbol{B}_{21}$ and $\boldsymbol{B}_{22}$ are updated with $\boldsymbol{\delta} + \boldsymbol{b}$ instead of $\boldsymbol{\delta}$), it is therefore also nonlinear with respect to the parameter vector $\boldsymbol{\theta}$.

We propose the application of SQP to solve the constrained nonlinear problem. Due to the complexity of the SQP algorithm and the positive semi-definiteness of the square matrix $\boldsymbol{b}$, we introduce a preprocessing algorithm (see algorithm 1) to trim a constant NLOS bias from the matrix $\boldsymbol{b}$. The algorithm mitigates a constant NLOS bias value b_c if all biases $b_{ij} \in \boldsymbol{b}_\theta$ satisfy the condition $|b_{ij}| \geq |b_c|$. From algorithm 1, the bias value b_c is initialized to zero and incremented with *step*, repeating the computation of error e_a at each iteration until it no longer decreases. It is important to set a value of *step* that is sufficiently small to allow the algorithm to reach the minimum as close as possible, without overshooting too quickly. The algorithm performs most effectively when all between-sets distances are affected by approximately the same amount of NLOS bias. Otherwise, it will trim off small measurement noise or return after the first iteration if any of the distances is unbiased.

Regarding the complexity of the SMACOF invocations applied in algorithm 1, one of the ways we speed up the convergence of SMACOF is to initialize only the first computation for $\boldsymbol{X}_t^{(0)}$ with a random array. Subsequent $\boldsymbol{X}_t^{(k)}$ computations are initialized with $\boldsymbol{X}_t^{(0)}$ or $\boldsymbol{X}_t^{(k-1)}$. The same applies to SMACOF computations for $\tilde{\boldsymbol{X}}_a^{(k)}$, which are initialized with $\boldsymbol{X}_a$ or $\tilde{\boldsymbol{X}}_a^{(k-1)}$. These initializations generally make SMACOF converge in constant time $\mathcal{O}(1)$.

Algorithm 1 Trimming NLOS bias from distances

Input: $\boldsymbol{X}_a,\ b^U,\ step$
Output: $\boldsymbol{X}_t,\ b_c$
Initialization : $b_c \to 0$
$\boldsymbol{X}_t^{(0)} = \texttt{MDS}(\boldsymbol{X}_a,\ b_c)$
$\tilde{\boldsymbol{X}}_a^{(0)} = \texttt{MDS}(\boldsymbol{X}_t^{(0)},\ b_c)$
compute $e_a^{(0)}$
$k \to 0$
while $k = 0$ **or** $e_a^{(k)} < e_a^{(k-1)}$ **do**
  $b_c = b_c + step$
  $k = k + 1$
  if $(b_c \geq b^U)$ **then**
    break
  end if
  $\boldsymbol{X}_t^{(k)} = \texttt{MDS}(\boldsymbol{X}_a,\ b_c)$
  $\tilde{\boldsymbol{X}}_a^{(k)} = \texttt{MDS}(\boldsymbol{X}_t^{(k)},\ b_c)$
  compute $e_a^{(k)}$
end while
$b_c = b_c - step$ {reverse last update}
$\hat{\boldsymbol{X}}_t = \texttt{MDS}(\boldsymbol{X}_a,\ b_c)$

The SQP algorithm as shown in algorithm 2 is then run on the constrained

nonlinear problem defined by eq. (4.5) and eq. (4.6). The implementation of the optimization algorithm makes use of Python-SciPy's SLSQP (Sequential Least Squares Programming) solver. The solver applies the Hans-Powell quasi-Newton method [78] for the derivative of the Lagrangian associated with the minimization problem in eq. (4.5) with a Broyden-Fletcher-Goldfarb-Shanno (BFGS) update. All the elements b_{ij} of this matrix are initialized with the constant bias value b_c. Afterwards, a matrix $\boldsymbol{U}$ composed by uniformly distributed values in $[0, 1)$ and with the same dimensions as $\boldsymbol{b}_\theta$ is added to $\boldsymbol{b}_\theta$. This is done to apply small perturbations to the initial values, which is known to provide better results than initializing all elements with the same value. The function f_e updates the value of e_a at each iteration within the SQP procedure while *tol* specifies the tolerance of the stopping criterion.

Algorithm 2 NLOS bias mitigation by SQP

Input: $\boldsymbol{X}_a,\ b_c,\ tol$
Output: $\boldsymbol{X}_t,\ \boldsymbol{b}_\theta$
Initialization : $\boldsymbol{b}_\theta^{(0)} \rightarrow b_c + \boldsymbol{U}[0, 1)$
1: $\boldsymbol{X}_t^{(0)} = \texttt{MDS}(\boldsymbol{X}_a,\ \boldsymbol{b}_\theta^{(0)})$
2: $\boldsymbol{b}_\theta = \texttt{SQP}(f_e,\ \boldsymbol{b}_\theta^{(0)},\ \boldsymbol{X}_t^{(0)},\ \boldsymbol{X}_a,\ tol)$
3: $\hat{\boldsymbol{X}}_t = \texttt{MDS}(\boldsymbol{X}_a,\ \boldsymbol{b}_\theta)$

4.2.2 Deployments with less than 3 tags

When the number of tags is $m = 1$ or $m = 2$, eq. (4.1) can not be applied directly for the computation of tentative anchor positions since at least 3 fixed nodes are required in order to produce unique solutions.

To overcome the lack of sufficient tags, the tag configuration is padded with some anchors from the anchor configuration so the number of tags makes up to 3. For example, in the case there are only two tags, we pad with one anchor. To ensure that all anchors participate in the padding and an error value can still be taken from tentative anchor positions, we apply a modified form of the jackknifing technique adopted in [20]. Anchors are sampled without replacements or ordering, taking $3-m$ anchors at each sampling step. Afterwards, the sampled anchors are added to the tag configuration so that the number of tags plus the anchor(s) becomes equal to 3. Tentative positions for the anchors left in the configuration after the samples have been acquired are computed using the augmented tag configuration. This process of sampling/jackknifing and computing of tentative positions is repeated for all possible combinations of anchors in the anchor configuration. Errors are computed

and stored, and all the errors are later summed into a final tentative anchor positions error e_a as described by the following equation:

$$e_a = \sum_{i=1}^{s} e_{a(i)}(\boldsymbol{X}_{t(i)}^{aug},\ \boldsymbol{b}) \tag{4.7}$$

The i^{th} augmented tag configuration $\boldsymbol{X}_{t(i)}^{aug}$ is defined by:

$$\boldsymbol{X}_{t(i)}^{aug} = \left[\boldsymbol{X}_{t}^{T} | \boldsymbol{X}_{a(i)}^{T}\right]^{T} \tag{4.8}$$

where $\boldsymbol{X}_{a(i)}$ is the i^{th} anchor sample(s) of size $(3-m) \times 2$ for 2D or $(3-m) \times 3$ for 3D positioning. The number s appearing in eq. (4.7) is the number of unordered combinations without replacement possible with the given number of anchors and tags and is defined by:

$$s = \binom{n}{3-m} \tag{4.9}$$

For instance, in a setup of 4 anchors and 1 tag, 6 anchor combinations are possible, allowing for 6 different augmented tag configurations.

As with the previous scenario with at least 3 tags, NLOS biases are first trimmed using algorithm 1 after which the final bias values are computed using algorithm 2.

4.3 Experimental Results

The experiments were performed using nanoLoc transceiver nodes in the laboratory environment shown in fig. 4.4b. The environment was not adjusted whatsoever for the sake of the localization exercise. This had the benefit of allowing RF interference from the multiple wireless devices in the environment and possible occlusions and reflections from nearby walls and objects. Data collected during the experiments and code used to process the data and visualize the plots are available online [54].

A nanoLoc node is shown in fig. 4.4a. The nodes use RT-ToF for estimating the ranges that are collected by the tags and sent via a base-station to a computer where, in turn, the distance matrix is constructed and node positions are calculated.

The nanoLoc nodes are mounted on tripods, as shown in fig. 4.4b. There are 4 anchors and a varying number of tags, from 1 to 4. The tags are kept stationary and an obstacle (shown in yellow in fig. 4.4b) is placed directly in front of anchor 3. This obstacle causes the distances between anchor 3 and all the tags to be approximately doubled. Variations in the tag positions in fig. 4.5b are directly explainable by small perturbations in the distance measurements taken by the transceivers leading to random hops within the MDS algorithm. A technique for dampening these hops

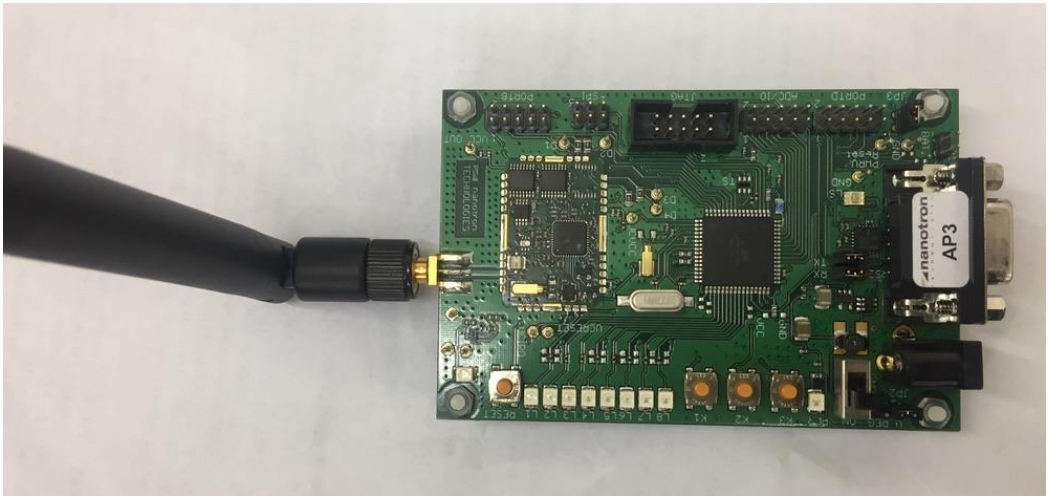

(a) The nanoLoc node used in the experiments.

(b) Deployment of 4 anchors (blue) and 3 tags (red) with an artifical obstacle (yellow).

Figure 4.4: Localization setup in a laboratory setting.

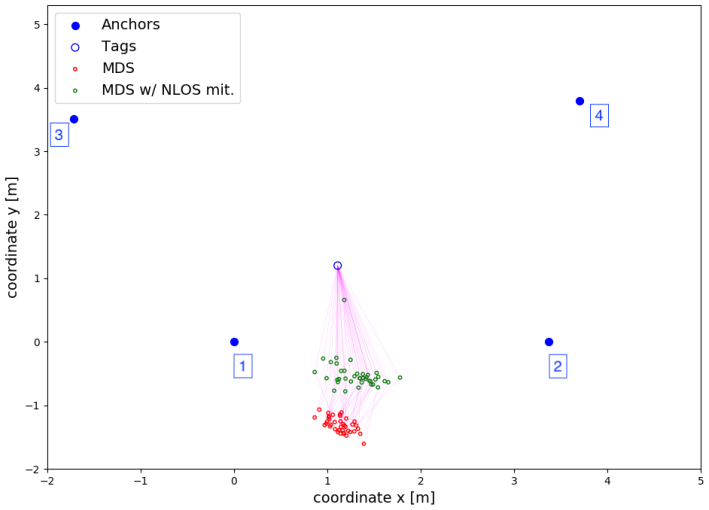

(a)

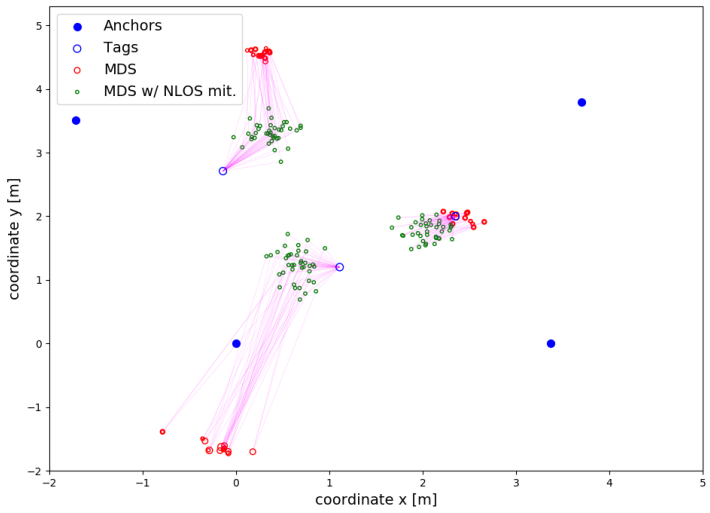

(b)

Figure 4.5: Positioning for 1 (a) and 3 (b) stationary nanoLoc tags with 40 data points per tag.

Table 4.1: Mean and variance of RMSEs for different nanoLoc tag counts.

No. of tags	MDS	MDS w/ NLOS mit.
	mean/var. (m)	
1	2.51/0.01	1.76/0.05
2	3.71/0.01	3.18/0.02
3	2.67/0.13	1.94/0.52
4	2.84/0.03	2.24/0.01

with respect to the MDS scheme has been discussed in [22]. The method takes into account the velocity of the nodes and applies MDS over a number of distance matrices contiguous in time. Usually, the method is applied for 2 contiguous matrices.

Table 4.1 shows the mean and variance of RMSE values for vanilla MDS and proposed method. The RMSEs at 2 tags and 3 tags are not correlated as a different version of the NLOS mitigation technique was applied for both scenarios, i.e., algorithm 1 and algorithm 2 respectively. We notice that in fig. 4.6a, around RMSE values of $3m$ on the Y-axis, the NLOS bias mitigation results are occasionally slightly worse than the original. We believe this is due to approximation errors in algorithm 1 and/or algorithm 2 and can be corrected by setting the *step* in algorithm 1 to a smaller value or reducing the tolerance value *tol* in algorithm 2. Decreasing the value of these parameters to provide fractional improvements in accuracy increases the time it will take for both algorithms to converge. The increase in RMSE in fig. 4.6a is due to a shift of the barrier closer to anchor 3. Human movements within the deployment region also create sudden spikes or dips. The histogram and empirical cumulative distribution function (CDF) for the RMSEs are reported in fig. 4.6b and fig. 4.6c.

4.3.1 Further Simulations

To verify the performance of our proposed method compared to vanilla MDS on a larger setup, simulations were performed to allow scaling up of the number of nodes and an expansion of the area of the deployment region. We initialize a rectangular $35m \times 25m$ simulated area with varying number of anchors and tags at random positions. Distance matrices with elements δ_{ij} are constructed from the pairwise distance between all the nodes and then tag within-sets distances are marked as unknown. The simulation ranging dynamics were modeled according to range estimation accuracy data provided in [3, 16], where NLOS bias is reported to approximate an exponential distribution while the measurement noise is modeled as

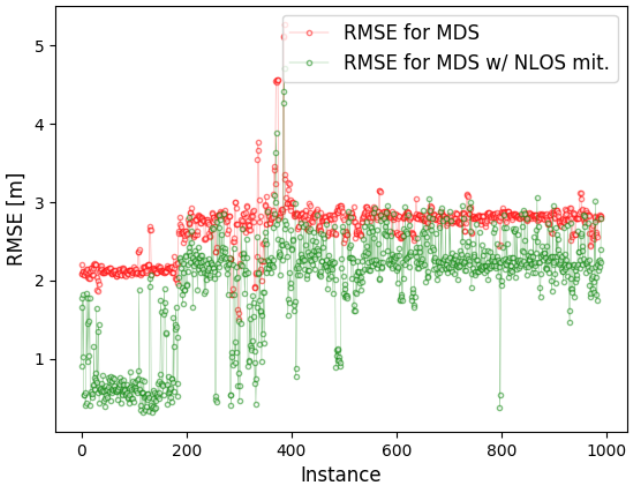

(a)

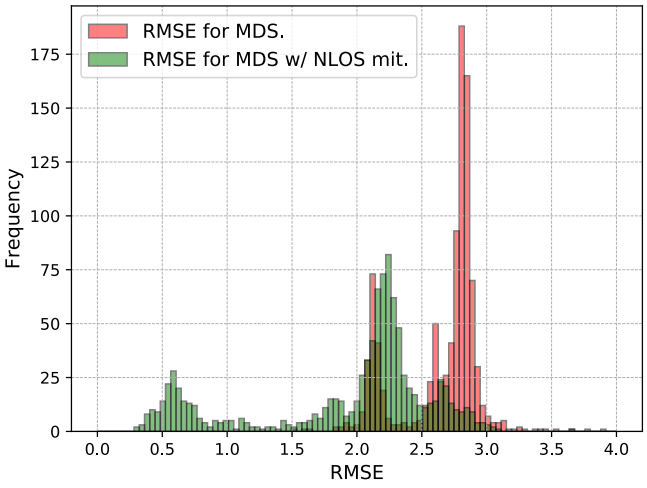

(b)

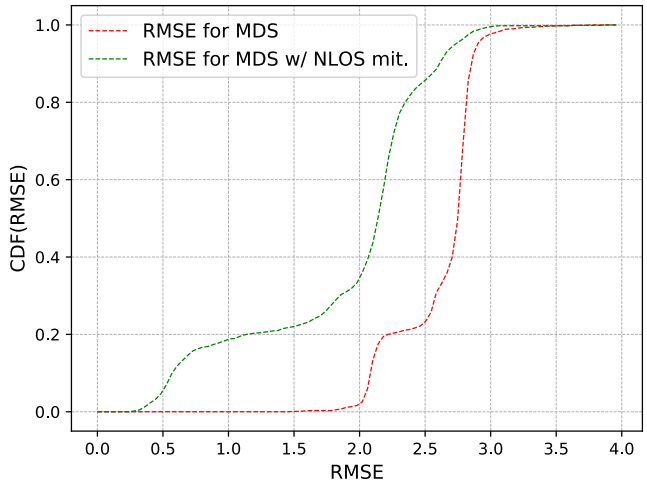

(c)

Figure 4.6: a) RMSEs; b) histogram of RMSEs; and c) CDF of RMSEs for 4 nanoLoc anchors and 3 tags with ≈ 1000 runs.

a zero mean Gaussian distribution. For ToF, the exponential distribution for NLOS bias $b_{ij} = Exp(\lambda)$ has scale $\lambda = 0.08\delta_{ij}$ and the noise $n_{ij} = \mathcal{N}(0, \sigma^2)$ has a standard deviation $\sigma = 0.02\delta_{ij}$ [3]. These values allow to inject the original distance δ_{ij} with some randomized NLOS and noise value so that the true distance d_{ij} is now related to δ_{ij} by:

$$\delta_{ij} = d_{ij}(\boldsymbol{X}) + b_{ij} + n_{ij} \tag{4.10}$$

Simulations were repeated for setups of 3 to 8 anchors and 3 to 22 tags. NLOS/noise multipliers are set in the range from 0 to 1. Anchors were placed at the four corners and midway between the four corners of the simulated area and tags were always initialized randomly within the rectangular bounds defined by the anchors.

Figures 4.7a to 4.7c show the results for the simulations where nodes and ToF dynamics were randomly initialized 500 times for each variation in the setup. The error in the position estimates is given by the RMSE of the computed tag positions with respect to the true tag positions. The median and IQR values for the 500 runs at each simulation are shown in the plots. From fig. 4.7a, the positioning RMSEs decrease as more anchors are added to the setup; tags were kept constant at 22 for this simulation set. This is because increasing the number of anchors increases the average magnitude of the error of tentative anchor positions, thereby allowing for a more robust inference on NLOS biases from the error. From fig. 4.7b, the number of anchors is kept constant at 4 while the number of tags is varied. This has the effect of increasing RMSE as tag count increases since information is lost as only 4 tentative anchor positions are reproduced from a relatively higher number of tags, with the NLOS mitigation approach always having a lower median value. In fig. 4.7c, we multiply the randomized b_{ij} and n_{ij} values by factors ranging from 0 to 1. Both the MDS and MDS-with-NLOS-mitigation approaches produce the precise tag positions when the multiplying factor is 0. As the factor is increased, the RMSE of our NLOS mitigation approach grows at a rate 0.7 that of vanilla MDS.

Summary

In this chapter, we presented an NLOS mitigation technique under the MDS-A scheme. This formed the basis for the more elaborate discussion on NLOS mitigation using recomputed anchor positions. An ideal matrix of pairwise distances is known to exhibit a symmetry that allows to recompute exact anchor positions from those tags using MDS. In a NLOS environment, this symmetry does not hold so that the

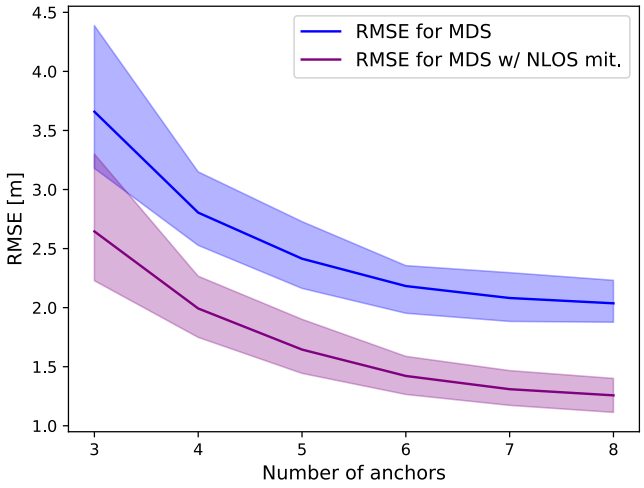

(a)

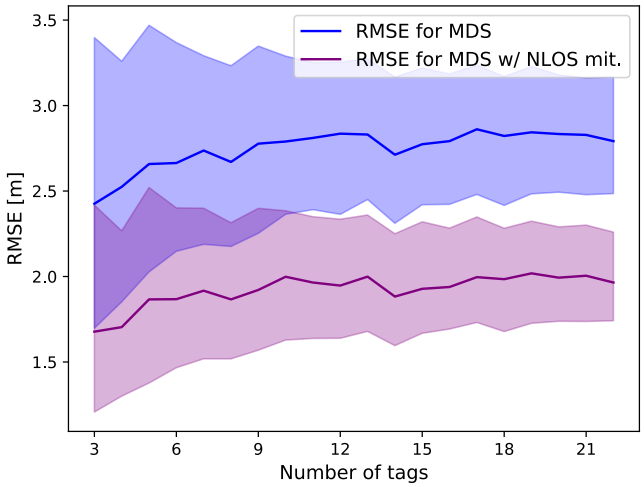

(b)

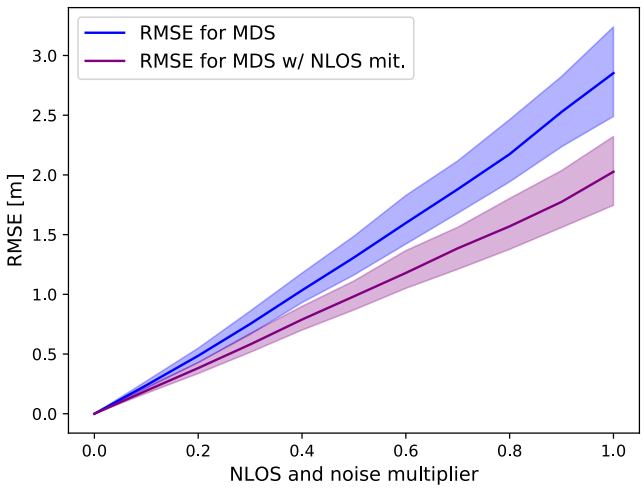

(c)

Figure 4.7: Medians and IQRs for RMSEs under a) varying number of anchors; b) varying number of tags; and c) varying NLOS and noise multipliers.

ensuing asymmetry can be exploited to estimate NLOS bias values for each of the pairwise distances.

We formulated a minimization problem where the error on anchor recomputation is presented as cost, and tag positions and NLOS bias are parameters to be optimized. An algorithm for the fast and global trimming of NLOS biases was first introduced, after which a SQP solution which computes per distance NLOS bias values was presented. The performance improvements of the proposed NLOS mitigation technique was validated by experiments with nanoLoc anchors and tags, and further on with simulations allowing for larger node deployments. Generally, results showed that positioning RMSEs can be decreased be reduced significantly with the cooperative NLOS mitigation here presented.

Chapter 5

Ranging under RSS Stochasticity

"In the face of ambiguity, refuse the temptation to guess."

Tim Peters

Range-based localization methods use range measurements to estimate the location of participating nodes in a localization scheme. The range can be estimated from properties that vary with distance such as time of travel of a RF signal in ToF [50] and TDoA [29], RF signal strength as in RSS [76] and magnetic field intensity as in magnetic field mapping [36]. Due to the ubiquity and availability of RSS on many wireless devices, it is commonly used to provide distance estimates for range-based localization. In most cases, the localization systems use RSS at short range where the distance estimates are more reliable or use RSS alongside other techniques such as ToF[72].

This is so, since RSS measurements have relatively high variance at long range and are strongly influenced by occlusions and interference in the deployment region of the RF devices. This chapter presents an overview of filtering techniques that can be used to process RSS readings in order to improve the accuracy of range computation from raw RSS with minimal computational overhead. The range estimates computed from the filtered data are compared with expected values of the perturbed range/distance expressed in terms of the CRLB for RSS-based distance estimation. Results show that filtering can significantly improve the accuracy of range estimation, highlighting the pros and cons of the presented filtering methods at different range values.

In the following sections, we introduce the RSS channel model, discuss the various filtering methods, examine the CRLB for ranging with RSS and conclude with experiments highlighting ranging improvements due to filtering.

5.1 RSS Channel Model

To estimate range from RSSI, the channel model – a mathematical representation of the effects of the channel as the RF signal propagates through it – is used to express the signal level at the receiver w.r.t the distance between the transmitter and receiver. The channel/path loss model expresses the shadow fading effect experienced by the signal for the traveled path. The shadowing gain/loss is usually reported as a log-normal random variable [41, 17, 75] from which the shadowing path-loss model in eq. (5.1) is derived which gives the power $\tilde{P}_{i,j}(\text{dBm})$ at the receiver and the shadowing gain/loss $S_{i,j}(\text{dBm})$. The average power $\bar{P}_{i,j}(\text{dBm})$ in relation to the actual distance $d_{i,j}$ is given by eq. (5.2).

$$\tilde{P}_{i,j}(\text{dBm}) = \bar{P}_{i,j}(\text{dBm}) + S_{i,j}(\text{dBm}) \tag{5.1}$$

$$\bar{P}_{i,j}(\text{dBm}) = P_0(\text{dBm}) - 10\eta \log_{10}\left(\frac{d_{i,j}}{d_0}\right) \tag{5.2}$$

The shadow fading effects are modeled by $S_{i,j}(\text{dBm})$ which is a random variable with Gaussian distribution $\mathcal{N}(0, \sigma_s^2)$ where σ_s is the log-normal spread. The average power $\bar{P}_{i,j}(\text{dBm})$ is expressed in terms of $P_0(\text{dBm})$ and d_0 which are power at and distance from a reference point respectively. The reference power $P_0(\text{dBm})$ is usually taken at $d_0 = 1m$. The constant η is the path loss exponent which is a property of the path/channel.

The actual distance $d_{i,j}$ between transmitter j and receiver i is the euclidean distance between transmitter coordinates (x_i, y_i) and receiver coordinates (x_j, y_j) given by eq. (5.3).

$$d_{i,j} = \sqrt{(x_i - x_j)^2 + (y_i - y_j)^2} \tag{5.3}$$

The perturbed distance $\tilde{d}_{i,j}$ to be estimated from the lossy power measurement can be expressed as a function of $\tilde{P}_{i,j}$ as shown in eq. (5.4).

$$\tilde{d}_{i,j} = d_0 \cdot 10^{\left(\frac{P_0 - \tilde{P}_{i,j}}{10\eta}\right)} \tag{5.4}$$

Henceforth, the RSS expressed in decibel-meter may be stated without adding the SI unit dBm as in eq. (5.4). Also, RSS and RSSI will be used interchangeably.

5.2 Measurement and Filtering Techniques

In this section, we describe the procedure for the measurement of RSSI and we discuss the various filtering techniques applied to the measurements. We only consider static

nodes for our measurements since channel properties evolve with the dynamics of the environment, and movements of RF nodes will require an online estimation of the channel properties as in [72], which is not part of the scope of the proposed discussion. More so, the variance of the measurements can easily be assumed to be invariant for static nodes for a not too large time duration.

5.2.1 Measurement setup

Two different sets of measurements were taken for the collection of RSS data. The first set of RSSI measurements were taken using COTS Bluetooth devices. The choice of Bluetooth as medium of communication has been made since the devices to be localized are moved to new fixed positions after measurements have been taken for the required period of time for the current position. Thus, they have to be powered with batteries, leading to a requirement of energy efficiency. The devices used in this measurement phase are classified into three roles: *tag*, *anchor* and *master*, where the *master* device which thus far has not been defined is now described as follows:

- **Master**: the master device plays the role of coordinating the group. It is a single device that gathers all the information from the other devices thereby acting as sink device and processing the measurement data. As a consequence of its role, it should be equipped with a powerful CPU to carry out the necessary computations.

For both tag and anchors, *Raspberry Pi 3* devices were used, since they are equipped with both WiFi and Bluetooth connections. As master device, instead, a Lenovo IdeaPad Y700 laptop was used. Two of the anchor and tag devices used for collecting our first category of RSS measurements are shown in figs. 5.1a and 5.1b while fig. 5.1c shows an example layout for the placement of tag, anchors and the master device.

The second set of measurements were taken using two nanoLoc transceivers where one is used as anchor and the other as tag. The RSS data for the tag device is read on the anchor device and sent to a sink device (similar to the master device for the COTS setup). The sink device is a desktop computer visible on the right in the background of the setup shown in fig. 5.2, with the anchor connected via the white serial cable.

5.2.2 Filtering techniques

In this subsection, we present the filtering methods that have been applied for preprocessing RSS measurements so they can be usable for range estimation. Some

(a) Anchor device.

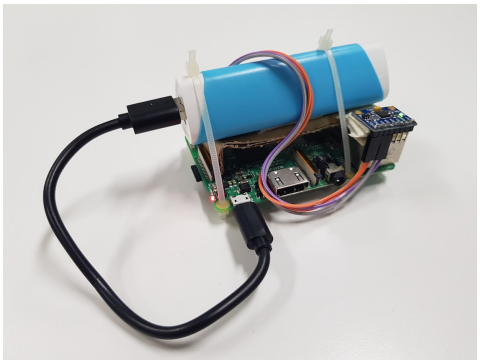

(b) Tag device.

(c) Basement with setup of tag and anchors.

Figure 5.1: (a) and (b) show anchor and tag Raspberry devices with mobile power supplies. (c) shows a typical setup of the devices.

Figure 5.2: Anchor and tag nanoLoc transceivers mounted on tripods each set at an height of 1.6m.

of the presented methods may have existing modified and improved versions. However, we limit our selection to the basic forms, which concomitantly, smoothen RSS with relatively small computational overhead and can be used in a real time localization context.

The independent variable is the measurement r_t in a time series of RSSI samples $\{r_t|t \in T\}$ at a time instance t. The state space is composed by the distance of the tag from the anchor which is parameterized by the path loss exponent η.

Simple Moving Average

A moving average (also known as rolling mean) filter creates a new sequence of data points by taking weighted averages of subsets of the data. The data subset is usually of fixed length and new subsets are created by adding a new point from the original data while excluding the oldest data point(s). A simple moving average (SMA) filter simply assigns equal weights to all the data points. In RSSI filtering, when samples do not share any notion of relative importance, all their weights can be considered the same, and a simple moving average filter can be applied.

For a time series of RSSI samples $\{r_t|t \in T\}$, at a given time instance t, the output sequence of the SMA filter using a window length n is given by eq. (5.5).

$$r_{sma} = \begin{cases} undefined, & 1 \leq t < n \\ \\ \frac{1}{n}\sum_{i=0}^{n-1} r_{t-i}, & t \geq n \end{cases} \tag{5.5}$$

The SMA sequence is undefined from start up to the window length n since the number of points are yet not sufficient to compute an average under the specified window length. SMA has the advantage of being relative easy to compute for successive time instances when a previous average is available, as shown in eq. (5.6).

$$r_{sma} = r_{sma[prev]} + \frac{r_t - r_{t-n}}{n}. \tag{5.6}$$

Exponential Moving Average

The exponential moving average (EMA) filter is another moving average filter which unlike the SMA applies exponentially decreasing weights to old data points. The weights decrease but never reach zero. Also, unlike the SMA which requires a few samples of size equal the window length to be initialized, the EMA can have its initial value set to the first RSSI value in the original stream while subsequent values are taken by summing the previous mean multiplied by a weight and the current

value multiplied by a different weight. The weight values are between 0 and 1, and both sum up to 1. Computation of the EMA is summarized by eq. (5.7).

$$r_{ema} = \begin{cases} r_t, & t = 1 \\ \\ \alpha r_t + (1-\alpha) r_{ema,prev}, & t > 1 \end{cases} \tag{5.7}$$

Since EMA filters do not filter using window sizes, in order to consolidate the idea of using a window size as with other filtering techniques, a decay parameter α is typically set following eq. (5.8).

$$\alpha = \frac{2}{n+1} \tag{5.8}$$

More so, since EMA never completely forgets old values, they are not very applicable to environments where the dynamics are changing rapidly such as nodes in motion where old measurement up to a certain limit are irrelevant.

Moving Median

The moving median filter similar to the moving average filter creates a new sequence by moving a window across the original data, and taking the median of the points captured by the window. Using a odd window size, the filter selects as output the median from the set of points in the window, which is a member of the set. This is not always the case for the moving average filter, since the computed average is not necessarily a member of the data points. More so, since the moving median 'sorts and select', it is less skewed by sudden spikes as compared to moving average since the magnitude of the spike does not contribute to the final outcome of the filter. The observation window can be centered at the sample point, so the filter output can track more precisely the original sequence. This implies waiting for the RSSI stream to produce $\frac{n}{2}$ more samples instead of n samples. The computation of a new point using moving median without centering is given by eq. (5.9).

$$r_{med} = \begin{cases} undefined, \ 1 \leq t < n \\ \\ MEDIAN(r_{t-n}, ..., r_t), \ t \geq n \end{cases} \tag{5.9}$$

Moving Mode

The moving mode filter like the moving average and median filters creates a new sequence of data by moving a window across the original sequence and taking the mode from all the points captured by the window i.e. the measurement that occurs

most frequently. From an accuracy point of view, the moving mode filter will perform better for unimodal RSSI distributions which are more frequent in line-of-sight (LOS) environments. However, RSS distributions aren't always unimodal, and in cases where the distribution of RSSI is multi-modal, the filter selects the dominant mode with the higher frequency if one exists.

The computation of a new point using the moving mode filter is given by eq. (5.10).

$$r_{mode} = \begin{cases} undefined, \ 1 \leq t < n \\ \\ MODE(r_{t-n}, ..., r_t), \ t \geq n \end{cases} \tag{5.10}$$

The new sequence has a time shift of n which can be reduced by applying the centering technique discussed in section 5.2.2.

5.3 Cramér-Rao bound for RSSI range estimation

Given an estimation problem and the best possible estimator, the CRLB expresses a lower bound for the variance of the unbiased estimates of an unknown but deterministic parameter. In our case, the parameter θ to be estimated is the range $\tilde{d}_{i,j}$ between transmitter and receiver w.r.t available RSSI measurements. The CRLB is known to be the reciprocal of the Fisher information [80] where the Fisher information $I(\theta)$ in this scenario is defined by eq. (5.11).

$$I(\theta) = -\mathrm{E}\left[\frac{\partial^2 \ell(\theta|\tilde{P}_{i,j})}{\partial \theta^2}\right] \tag{5.11}$$

The log likelihood function $\ell(\theta|\tilde{P}_{i,j}) = \ln f_\theta(\tilde{P}_{i,j})$. Since the shadowing losses have been described as log-normal in eq. (5.1), the measured power $\tilde{P}_{i,j}$(dBm) can therefore be described as being of Gaussian distribution $\mathcal{N}(\bar{P}_{i,j}, \sigma_s)$ so that the probability density function $f_\theta(\tilde{P}_{i,j})$ at $d_0 = 1$m is as shown in eq. (5.12).

$$f_\theta(\tilde{P}_{i,j}) = \frac{1}{\sqrt{2\pi\sigma_s^2}} \cdot \exp\left\{-\frac{1}{2\sigma_s^2}(\tilde{P}_{i,j} - \bar{P}_{i,j})^2\right\} \tag{5.12}$$

The log likelihood $\ell(\theta|\tilde{P}_{i,j})$ becomes:

$$\ell(\theta|\tilde{P}_{i,j}) = \ln\left(\frac{1}{\sqrt{2\pi\sigma_s^2}}\right) - \frac{1}{2\sigma_s^2}(\tilde{P}_{i,j} - \bar{P}_{i,j})^2 \tag{5.13}$$

The second order derivative $\nabla^2_\theta \ell$ can be taken using the chain rule for second order derivatives:

$$\frac{\partial^2 \ell}{\partial \theta^2} = \frac{\partial^2 \ell}{\partial \bar{P}^2_{i,j}} \left(\frac{\partial \bar{P}_{i,j}}{\partial \theta} \right)^2 + \frac{\partial \ell}{\partial \bar{P}_{i,j}} \frac{\partial^2 \bar{P}_{i,j}}{\partial \theta^2}. \tag{5.14}$$

Each term in the differential equation in eq. (5.14) are easily solved:

$$\frac{\partial \ell}{\partial \bar{P}_{i,j}} = \frac{1}{\sigma_s^2}(\tilde{P}_{i,j} - \bar{P}_{i,j})$$

$$\frac{\partial^2 \ell}{\partial \bar{P}^2_{i,j}} = -\frac{1}{\sigma_s^2}$$

$$\frac{\partial \bar{P}_{i,j}}{\partial \theta} = -\frac{10}{\ln(10)} \cdot \frac{d_0}{d_{i,j}} \cdot \eta$$

$$\frac{\partial^2 \bar{P}_{i,j}}{\partial \theta^2} = \frac{10}{\ln(10)} \cdot \frac{d_0}{d^2_{i,j}} \cdot \eta$$

Following eq. (5.11), the expected value of each term is taken so that the first term becomes zero since $\mathrm{E}[\tilde{P}_{i,j}] = \bar{P}_{i,j}$ and the rightmost expression in eq. (5.14) equally becomes zero. Substituting the expected values of the rest of the differentials into eq. (5.11), and taking the reciprocal, we have an expression the CRLB which gives a lower bound on the ensemble variance of the range between transmitter j and receiver i for unbiased range estimated from raw RSS measurements in eq. (5.15) [79].

$$\mathrm{var}(\hat{\theta}) \geq \mathrm{CRLB} = \left[\frac{\ln(10)}{10} \right]^2 \cdot \frac{\sigma_s^2}{\eta^2} \cdot d^2_{i,j} \tag{5.15}$$

The value of the reference distance d_0 has been taken as 1m. This CRLB expression relies on the assumption that the environment is a LOS one and the estimator is unbiased[65]. Again, rearranging eq. (5.12), the mean for the estimated perturbed distance can now be expressed in terms of the CRLB as shown in eq. (5.16), in conformity with [75].

$$\mathrm{E}[\tilde{d}_{i,j}] = d_{i,j} \cdot \exp\left\{ \frac{1}{2} \cdot \frac{\mathrm{CRLB}}{d^2_{i,j}} \right\} \tag{5.16}$$

The expression in eq. (5.16) is the expected value of the perturbed distance $\tilde{d}_{i,j}$ when estimated by an unbiased estimator with maximal efficiency. This distance will be compared with those obtained using eq. (5.4) and the RSSI measurements

used for the distance estimations will be those obtained after applying the filters discussed in section 5.2.2.

5.4 Experimental results

In this section, we describe the experiments in which RSS data was collected and results of the filtering techniques discussed in section 5.2 are compared. As stated earlier, two categories of dataset were collected: 1) data from a COTS device (*Raspberry Pi 3*) anchor and tag 2) data from two nanoLoc transceivers used as anchor and tag. The dataset for the latter had a relatively lower variance due to the higher signal-to-noise ratio and the adopted Chirp Spread Spectrum modulation scheme which uses a higher bandwidth (one 80MHz channel and three 22MHz channels) with all of the bandwidth used to broadcast the signal as compared to the former which uses Bluetooth Low Energy technology with Direct-Sequence Spread Spectrum (40 2MHz channels).

In a LOS environment, the nanoLoc devices show unimodal distributions as shown in fig. 5.3 whose mode/median values are significantly distinct from every other value in the distribution. The RSSI values for the nanoLoc devices range from 0-63 and are mapped to power in dBm using a table of values provided by nanoLoc development user guide [1]. However, this is not the case for the measurements from the COTS devices – the *Raspberry Pi 3*s – with the histograms shown in fig. 5.4. The RSS distributions in this case do not indicate a prominent value over a period of time and as such might require some form of filtering to make the data useful for range estimation. The stride values of 2 to 3m between measurements for the COTS were chosen because the distributions were not significantly distinguishable at ranging strides of 1m.

The raw data at each range were filtered using the discussed filtering techniques and the filtered sequences are plotted as shown fig. 5.5 using a window size of 5 and then 15. The effect of an increased windows size is immediately evident from the figures as fluctuations in the filtered sequence are significantly reduced.

In table 5.1, the means and variances for the raw RSSI and filtered data shown in fig. 5.5b for a window size of 15 are summarized. The SMA has the least variance of all the methods while moving median has the least mean value. In order to estimate range from the RSSI and then estimate the CRLB value, the path loss exponent η and the log-normal spread σ_s are required. From table 5.1, we observe that σ_s is fairly constant with range, indicating that the RSSI distribution is nearly homoscedastic with respect to range. From the COTS devices dataset, we perform

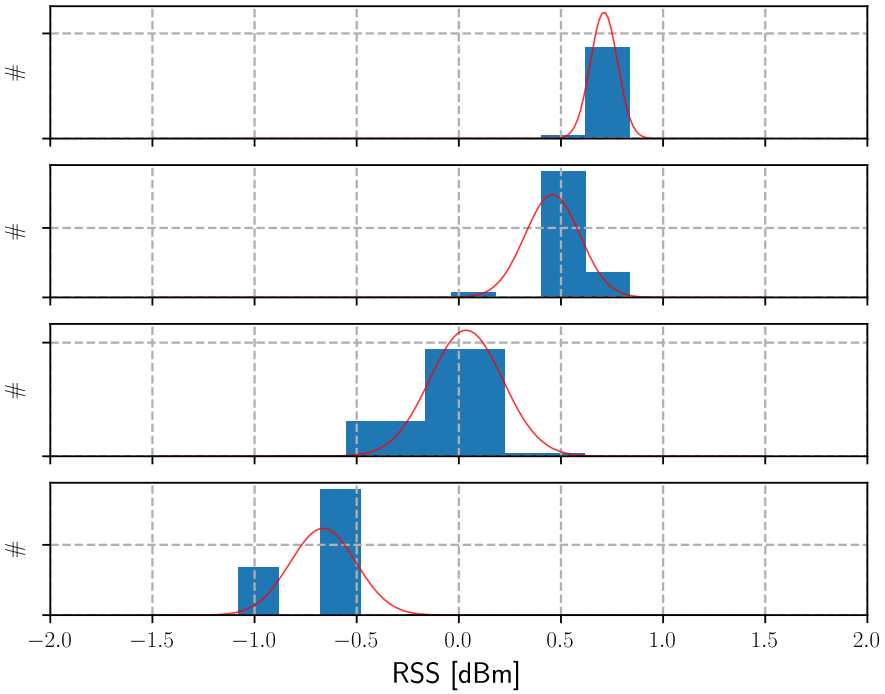

Figure 5.3: Histogram of RSS for nanoLoc anchor and tag at 2m (topmost), 3m, 4m and 5m apart in a LOS environment.

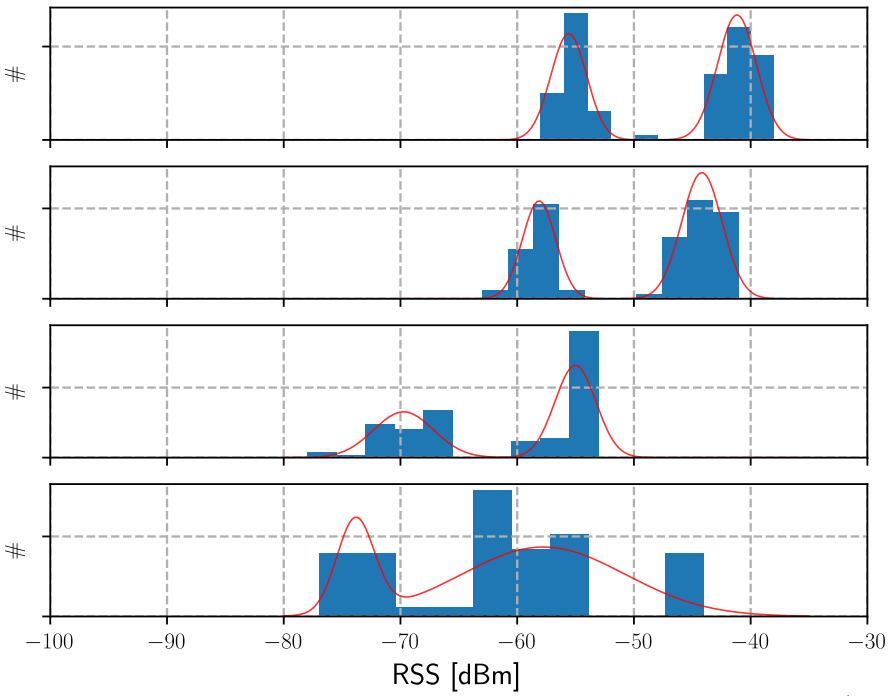

Figure 5.4: Histogram of RSS for COTS device anchor and tag at 2m (topmost), 5m, 7m and 10m apart in a LOS environment.

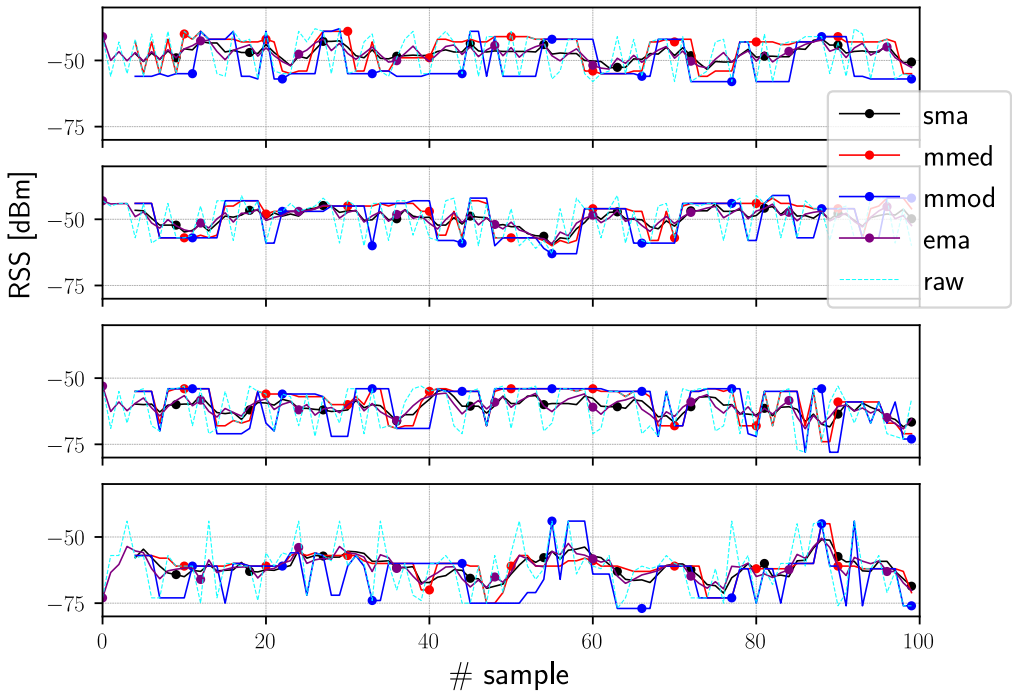

(a) At window size 5.

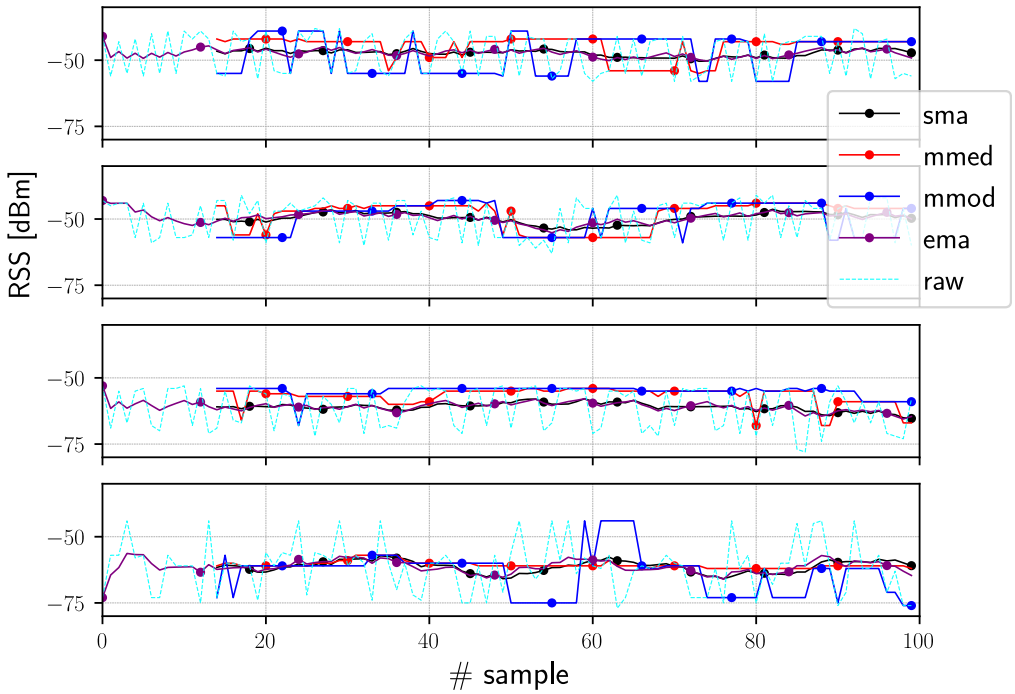

(b) At window size 15.

Figure 5.5: RSS for COTS device anchor and tag at 2m, 5m, 7m and 10m apart in a LOS environment.

Table 5.1: Statistics for raw and filtered RSSI with sample size 100 and window size 15.

d (m)	Raw	SMA	EMA	MMED	MMOD
			mean/s.d.	(dBm)	
2	-47.5/7.3	-47.4/1.2	-45.5/4.8	-45.5/4.8	-47.9/7.3
5	-49.9/7.0	-50.1/2.0	-49.7/2.3	-49.4/5.2	-49.4/5.7
7	-60.5/7.2	-60.5/1.0	-60.3/1.4	-56. 0/2.0	-54.7/1.8
10	-61.5/8.9	-61.4/2.2	-61.5/2.6	-60.4/1.3	-62.3/8.4

Table 5.2: CRLB and expected $\tilde{d}_{i,j}$ values at window size 15.

	2m	5m	7m	10m
CRLB (m^2)	2.75	15.75	32.61	100.99
$E[\tilde{d}_{i,j}]$ (m)	2.83	6.85	9.76	16.57

a fast estimation of the path loss exponent by fitting a linear regressor on the log of normalized distances $10\log_{10} d_{i,j}$ and average power $\bar{P}_{i,j}$(dBm) at each range in the measurements. Distances were normalized at $d_0 = 1m$, yielding $\eta = 2.03$ and $P_0 = -39.60$ dBm. We compute different CRLB by eq. (5.15) for each range using the spread value at the range and compute the expected perturbed distance value $\tilde{d}_{i,j}$ by eq. (5.16) for each range. The CRLB and $E[\tilde{d}_{i,j}]$ values are summarized in table 5.2.

With η and P_0 known, range values are computed using eq. (5.4) to compare estimates from the raw RSSI data with the expected value of perturbed distance $E[\tilde{d}_{i,j}]$ and the range values from the filtered RSSI data. The ranging errors (computed distances$-$actual distances) for each of the methods are plotted in fig. 5.6 at window size values of 5 and 15. The error of the expected value of the perturbed distance is plotted alongside the filtered outputs to better visualize the statistical impact of filtering.

Empirical CDFs of the absolute value of the ranging errors for each of the filtering methods and original measurements are shown in fig. 5.7 for window sizes 5 and 15. From the CDF plots, we observe that at all times, all the filtering methods except the moving mode filter perform better than the distances computed from the raw RSSI measurements. More so, the SMA and EMA sequences do not suffer from sudden fluctuations as with the moving median and moving mode methods. The moving mode method has the worst performance of all three because the distributions are not unimodal. The moving average methods – SMA and EMA – perform better at short

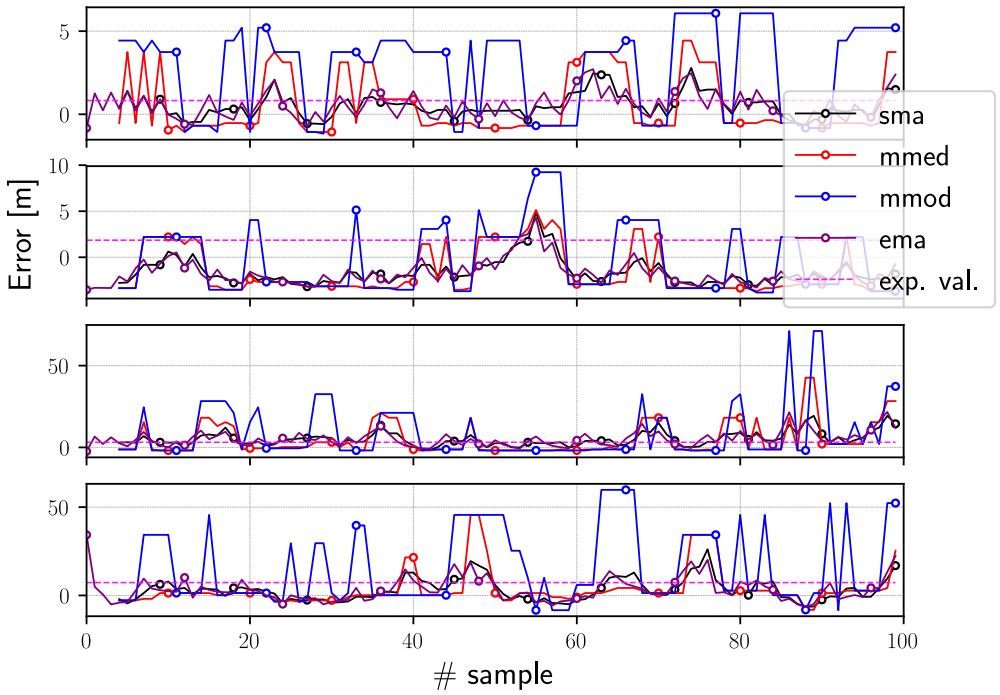

(a) At window size 5.

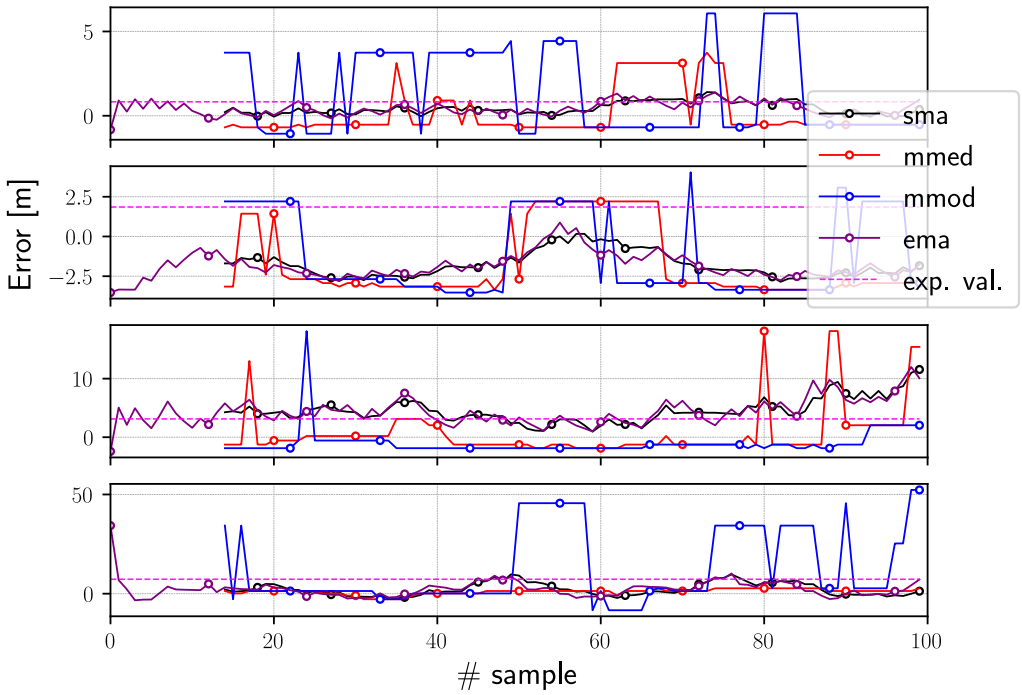

(b) At window size 15.

Figure 5.6: Ranging errors at 2m (topmost), 5m, 7m and 10m apart at window sizes 5 and 15.

range since a short duration of outlier measurements do not have an overwhelming advantage for relatively long windows. Such outlier measurements are however likely to emerge in the moving median filter depending on their duration and size of the window. The moving average methods are equally suitable for filtering at small window sizes and have lower time complexity as they can be computed in constant time $\mathcal{O}(1)$ as compared to moving median's average $\mathcal{O}(n)$ complexity (using *quickselect*) and moving mode's $\mathcal{O}(n)$ complexity.

5.4.1 Window Tuning

In fig. 5.8, the RMSEs of the generated sequences for each filter were plotted against different window size values starting from size 3 to size 20. From the figure, the RMSE values decrease as the window size value increases bearing in mind that the anchor and tag devices are static. The window size should however not be kept extremely large since the environment and hence channel properties change with time, and new RSSI readings may vary significantly from previous ones after a sufficiently large time frame.

For dynamic nodes, the window size should be parameterized by the relative speeds of the anchor and tag nodes such that the filter dynamics are always faster than those of the nodes.

Summary

In this chapter, we presented an overview of filtering methods that can be used to process raw RSSI data to make them more usable for the computation of range. SMA, EMA, Moving Median and Moving Mode were the candidate filtering methods and have been studied due to the low computational overhead required to use them for filtering RSSI streams in real-time. The discussed filtering methods were shown to be more applicable to data collected from COTS devices and have been studied within the context of static nodes deployed in LOS environments. Results show that the environment – LOS or NLOS – and participating RF nodes – COTS or specialized hardware – strongly influence the RSSI distributions and by extension the behavior of the filters. Filtering has shown to generally improve the accuracy of the computed range when compared to direct computation from the raw data. The SMA and EMA methods showed the best overall filtering performance over the set of studied ranges: 2m, 5m, 7m and 10m. Increasing the window size (up to a certain limit) has equally shown to provide improved ranging accuracy.

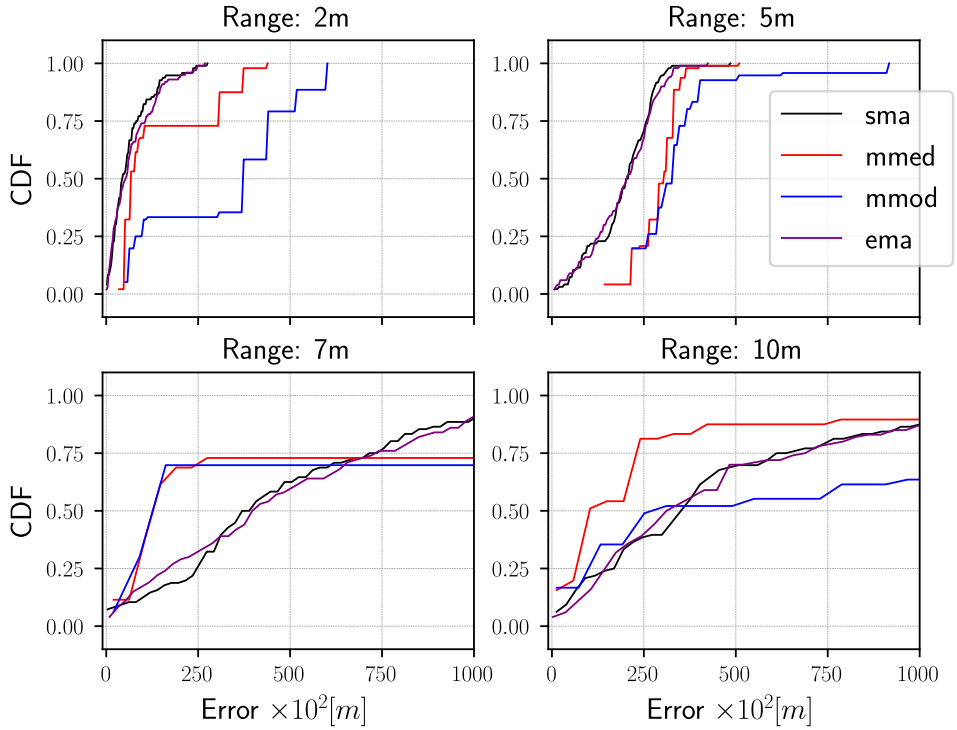

(a) CDFs of ranging error at window size 5

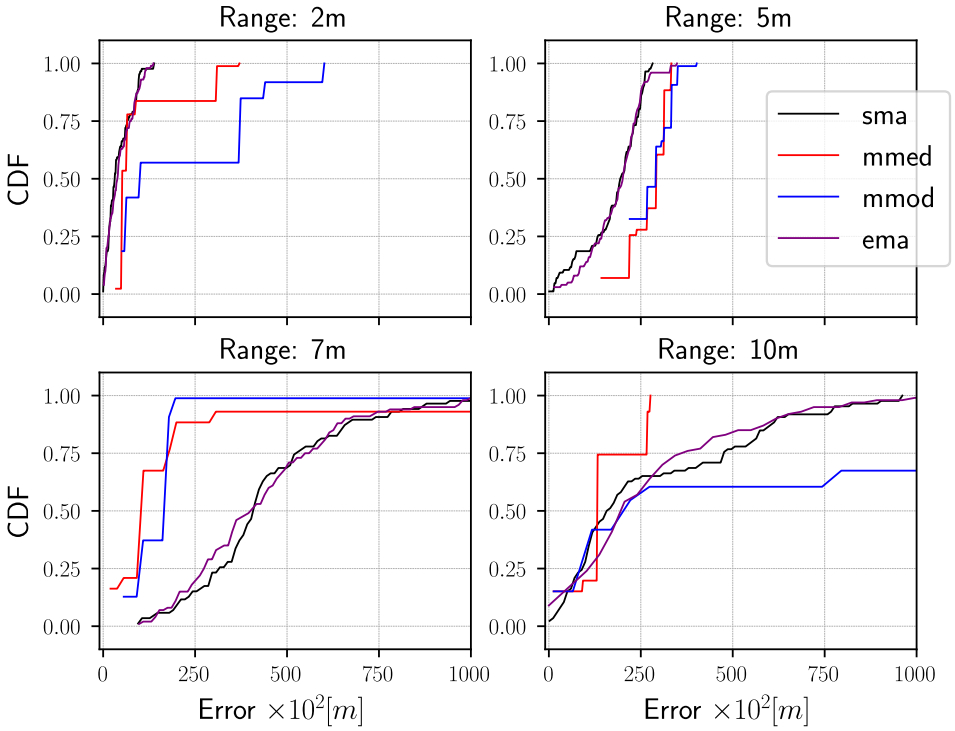

(b) CDFs of ranging error at window size 15

Figure 5.7: Empirical CDFs of absolute ranging errors.

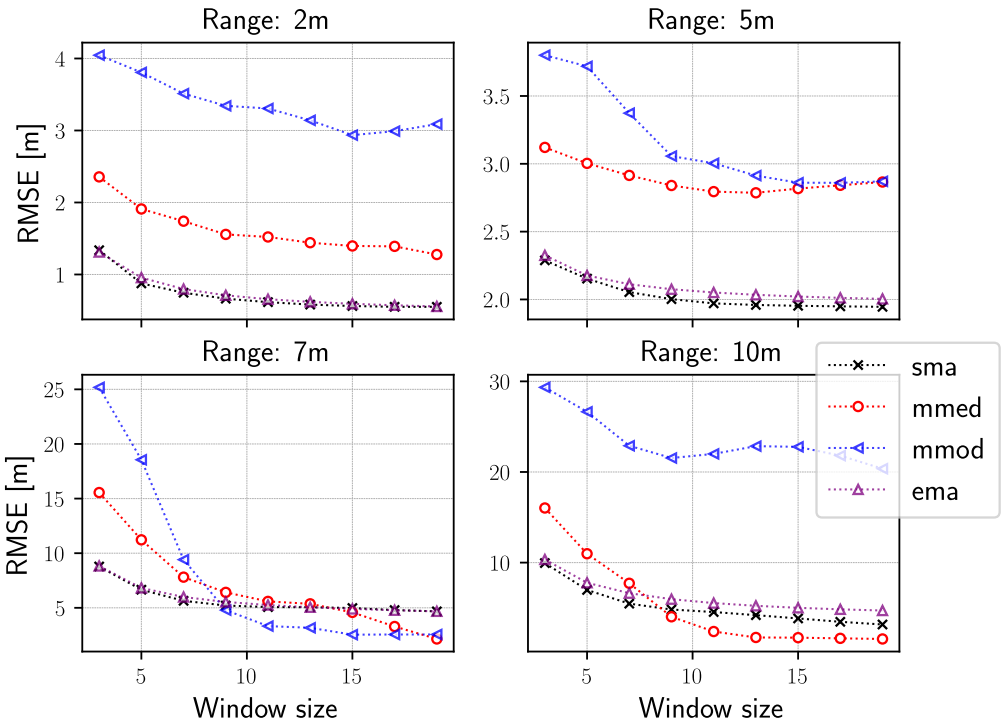

Figure 5.8: RMSEs of the filtering techniques under incrementing window sizes at different ranges.

Chapter 6

Design of Scalable Localization Systems

"The fantastic power and ultimate absurdity of unchecked exponential growth."

Geoffrey West

Scaling of localization systems has been studied in previous research to understand the theoretical limits of performance (accuracy and efficiency mostly) of various localization architectures and/or deployments. Design considerations addressed the number of anchors and anchors to tags ratio [27], integrability of existing techniques such as UWB two-way ranging (TWR) in practical scenarios such as Unmanned Aerial Vehicle (UAV) localization [91], partitioning of large-scale measurements into smaller and localized forms [107, 86] and reuse of low cost RF devices such as smartphones over custom nodes [89]. In addition to these, energy requirements are to be kept minimal as the deployment scales, which would often imply resorting to low energy wireless technologies such as Bluetooth LE and low-power UWB. A summary of the important considerations that we think influence our overall cooperative localization system design: architecture, data and mobility, are discussed in this chapter.

6.1 Architecture

The architecture of the deployment is at core of the localization system as it largely determines the extensibility and scalability of the system. It equally influences the constraints on communications between participating nodes and how the nodes are orchestrated in general. In the following sections, we discuss communication and node placement as relating to scalability.

6.1.1 Communication

The communication can either be simplex or duplex. Simplex implies one class of nodes (anchors or tags) transmit, while the other class receives. Duplex implies both anchors and tags are transmitting and receiving, i.e. nodes are implemented as transceivers. Defining how communication between nodes is coordinated is not trivial and will raise the following design questions: *Who transmits? Who receives? How fast can we communicate? How many nodes can communicate per time?*

Tags transmit, anchors receive

In this scenario, tags are synchronized via a global clock and transmit in turns to each anchor. For the scheduling of the transmissions, information can be sent in a TDMA fashion, such that each mobile node uses a predefined time slot to send its own localization data. Otherwise, tokens can be passed from one mobile node to another which can help reclaim unused bandwidth and eliminate TDMA synchronization overheads but with a penalty of extra computational load for the token passing mechanism. Either way, both approaches will degrade quickly as more nodes are added. For TDMA scheduling, a random node would need to wait $\Delta t \times (n-1)$ time for its own transmission window given n tags and an average time of Δt. To resolve this, the network can be partitioned by grouping tags with their nearest anchors to cut down TDMA latencies. This approach would create increased complexity through the final merging of local localization results and would require a sufficiently larger number of anchors to ensure tags are not orphaned with less than 3 nodes at any time.

Anchors transmit, tags receive

This is the conventional communication architecture applied in RSSI fingerprinting and propagation model estimation approaches. In the case of fingerprinting, the anchor nodes are can be Wi-Fi transmitters since they mostly have 100% uptime, as localization is a secondary application to their original Internet connectivity application. While this approach can be scaled to as many tags as possible, it requires the tags to compute their own location using supervised learning algorithms such as k-means or neural networks, which are computationally intensive. In the other case where distance is computed from RSS, tags need to recompute channel properties over time with the assumption that ground truth in the form of markers with known locations are available so that channel properties can be correctly estimated.

Anchors and tags are transceivers

From our experience, this is the most suitable communication architecture as it equally offers flexibility with the role anchors or tags play; they can transmit, receive or do both. More so, since tag and anchor hardware is now homogeneous, the role of any node can be swapped from anchor to tag and vice-versa. The communication is usually organized such that anchors transmit and tags receive and re-transmit back to anchors. In this way, the heavy processing can be done by anchors or, even better, by a "concentrator" or "sink", which is a sufficiently powerful machine and receives information from all the anchors via a wired or wireless connection. Heavy processing on nodes would be tolerable for mobile robots (although not always) but not for tags mounted on regular objects or humans – processing would be deferred from the tag to a more powerful device. Data sent back from the tags can easily include RSSI, inertial measurements and any other useful information. Clock sync between anchors may not be needed, depending on the type of processing that is done by the sink (e.g., it should not be needed for using RSS; for ToF it is instead required). The sync could be done by the sink once the schedule of the communications is known.

6.1.2 Node Placement

In tightly congested deployments, the probability of having occlusions increases significantly. The ratio of NLOS to LOS measurements can therefore be roughly described in terms of the average number of tags per unit area and the number of anchors nodes. The more anchor nodes there are, the higher the likelihood of getting a LOS for each tag. Therefore, accuracy can be kept fairly constant as the number of tags increases, if the number of anchors is increased proportionally or the deployment area is expanded. However, the latter is mostly infeasible and impractical for most scenarios. It is also relatively much easier to add more anchors than expand the area.

Where should the anchors be placed? Placing them on the same plane as the mobile nodes is the intuitive answer but does not provide for minimum NLOS to LOS ratio. The anchors should be placed high above the tags such that the likelihood of creating an occlusion between a tag and anchor by another tag is reduced. The positions are then computed using a 3D localization algorithm; in our case, this is easily achieved by changing the dimension P of the MDS procedure for MDS-based localization. An equidistant spacing of anchors is suitable for open areas where mobile nodes can travel freely, while the addition of more anchors to areas with crowded objects and/or fixed obstacles will be more suitable for office settings.

6.2 Data

Collection of measurements is an important part of localization. Mixing of various measurement sources does make for a reduction in the latency of new available measurements. As discussed in chapter 2, solutions combining various data sources such as RSS and ToF compensate the inaccuracy or computational cost of one source using the complementary features of the other source. The rate at which measurements are collected/data is collated determines the frequency with which new location data is published.

How fast can these measurements/data be collected/collated? This question is addressed in the following sections.

6.2.1 Generating Data

In the primary RF data sources we considered in this work – ToF and RSS, data is generated by either sampling the RSS value of an active node in multicast mode or pairing nodes to measure time of travel between the nodes. A node's RSS value can be read by a large amount of listening nodes simultaneously, although it is impossible to pair a node with more than one node at one time to perform ToF ranging. Hence, with RSS, measurements are collected for as fast the listening node is able to sample. In the case of ToF, this rate depends on the slower clock speed of the pair. To improve the rate at which measurements are collected in large networks, all nodes can sample RSS of every other node (depending on the network interface card), while the same partitioning principle can be applied on the large network to allow for the more accurate ToF ranging between nodes.

6.2.2 Other onboard sensors available?

In the case IMU data or magnetic field intensity is available from sensors on the mobile node, they can be used to complement existing data from other sources and improve positioning accuracies. For the time between successive samples of RF signals, these data will be used for dead-reckoning allowing for a relaxation of the sampling time of RF signals and as a consequence, support for more nodes. A Kalman filter can be used to fuse the data from the different sources. The fusion can be performed on a remote device or on the tag device if it has sufficient computational resources.

6.3 Mobility

The likelihood of collisions between nodes or occlusion of one node by another increases with the relative speed between the nodes. These occlusions/collisions although transient can create temporary positioning ambiguities such as unrealistic jumps in estimated positions. For these reasons, a study of positioning under mobility becomes of interest as the number of nodes start to grow. Since node mobility is generally uncontrolled (i.e. stochastic) in practical scenarios, mobility can instead be simulated as a Gauss-Markov process to allow to test localization algorithms under large scale deployments. An Ornstein-Uhlenbeck process (a stationary Gauss-Markov process) can be used to simulate a Brownian motion-like mobility model. This motion model can be instantiated independently for each simulated node using thread or process level parallelism. The limit on the number of models that can be instantiated (which by consequence now determines the number of nodes) will depend on the multiprocessing capabilities of the machine on which the simulation is run.

Chapter 7

Conclusions

"Stay hungry, stay foolish."

Steve Jobs

Indoor localization is gaining superior relevance in many applications areas. This fact has increased research interests in the subject more recently. In this thesis, techniques relating to the mitigation of uncertainties for cooperative indoor localization were discussed. The motivation behind the development of this techniques is the apparent saturation and/or huge cost implications of hardware approaches that attempt to mitigate these same uncertainties. The addressed uncertainties include NLOS effects in the environment, stochasticity of the signal strength of RF signals, missing interaction between tags and management of dynamic node membership.

The introduced cooperative localization scheme uses MDS to place objects in a configuration of points given a joint matrix of pairwise distances. We proposed a specialised form of MDS that undermines missing data in the form of interaction between tags. The proposed form has significantly better accuracy than classical MDS and a slightly better accuracy than an existing method which attempts to recover such missing distances using the shortest path information.

To tackle the effect of NLOS, we formulated a constrained-optimization problem that exploits the intrinsic symmetry that allows to compute tag positions from anchors' and anchor positions from those of tags in a LOS environment. In an NLOS environment where this symmetry is lost, we quantify the asymmetry by taking the magnitude of the error on recomputed anchor positions. The optimization problem is parameterized by the optimal position and the amount of NLOS bias per distance. We described an SQP approach for solving this problem. From experimental results, we conclude that position errors can be reduced significantly using our mitigation technique: in a setup of 4 fixed anchors and 3 mobile nodes, a reduction of up to 28% was observed.

To improve the performance of ranging with RSS, methods for filtering signal strength measurements were examined for static nodes. Preprocessing in the form of filtering had been shown in earlier research to improve ranging results. Our study of filtering techniques further confirmed this. The considered filtering techniques were of low computational complexity, which can be adapted into WSN solutions without fear of significant energy requirements. The considered methods were SMA, EMA, moving median and moving mode. We compared the range values computed from filtered measurements with range values computed from raw measurements as estimated from an unbiased estimator via the CRLB. SMA and EMA showed the most promising result with the additional advantage that they can be computed in constant time $\prime(1)$ given a value from the previous time frame.

Dynamic node membership was trivially managed by a subroutine that collects pairwise distance information from the new node as it comes online and continuously pads the matrix with this info. Similarly, nodes that go offline were managed the same way; the rows and columns of the distance information corresponding to that node are sliced off or masked.

7.1 Future Work

Using our work as a starting point, there are areas we feel can enjoy provide further improvements. These areas are related to the common of goal of further improving positioning accuracy for cooperative localization under uncertainties and are considered in the following subsections.

7.1.1 Further Improvements to NLOS Mitigation

Removing NLOS bias completely is practically impossible. However, we can look further into more ways with which to improve the current NLOS mitigation technique. In the current approach, we only consider the magnitude of the errors of the recomputed anchor positions disregarding the directionality of the error vectors. We need to study the behavior of the error vectors of the recomputed anchor positions to properly understand how their direction correlates to the per-distance NLOS biases.

More so, we currently need to solve two optimisation problems – one for computing the position with MDS-A, and another for estimating NLOS bias effects in order to trim from the distances. It might be possible, however, to combine both optimisation steps into one to speed up the time required to perform the estimation of positions and NLOS biases, although this optimization of the process would only benefit

large scale deployments, since the current formulation of our solution is definitely applicable to small systems.

7.1.2 RSS Filtering for Non-Static Nodes

Our study on filtering techniques involved static nodes in order to understand signal strength variations with node mobility decoupled. No easier way to keep mobility decoupled than keep nodes static. However, in real applications, mobile nodes are mostly in motion and hardly ever static. Considering these, it would be of great interest to further study the already examined filtering techniques under controlled motion scenarios. We intuit that conditions such as node speed, acceleration, jitter and heading with respect to a pair node will influence the variance of RSS thus requiring a more adaptive approach to filtering, such as dynamic window sizes.

7.1.3 Simulating Motion

Integrating a suitable simulation model into our cooperative localization solution will help to carry out simulations to support some of the aforementioned further work proposals with simulations. This would allow to rapidly prototype localization deployments to test conjectures without having to setup real nodes and make exhaustive floor markings to work with mobility in real life. Such motion model can be a stationary Gauss-Markov process, which can be implemented with a simple Ornstein-Uhlenbeck process (discussed in chapter 6) to simulate Brownian motion-like movements.

Bibliography

[1] nanoLoc development kit user guide. *Nanotron Technologies GmbH, Berlin, Germany, Technical Report NA-06-0230-0402-1.03*, Feb 2007.

[2] A. A. Ahmed, H. Shi, and Y. Shang. Sharp: a new approach to relative localization in wireless sensor networks. In *25th IEEE International Conference on Distributed Computing Systems Workshops*, pages 892–898, June 2005.

[3] B. Alavi and K. Pahlavan. Modeling of the distance error for indoor geolocation. In *2003 IEEE Wireless Communications and Networking, 2003. WCNC 2003.*, volume 1, pages 668–672 vol.1, March 2003.

[4] Y. Bai, W. Jia, H. Zhang, Z. Mao, and M. Sun. Landmark-based indoor positioning for visually impaired individuals. In *2014 12th International Conference on Signal Processing (ICSP)*, pages 668–671, Oct 2014.

[5] Syagnik (Sy) Banerjee and Ruby Roy Dholakia. Location?based mobile advertisements and gender targeting. *Journal of Research in Interactive Marketing*, 6(3):198–214, 2012.

[6] David Barras, Frank Ellinger, and Heinz Jäckel. A comparison between ultrawideband and narrowband transceivers.

[7] P. Barsocchi, F. Furfari, P. Nepa, and F. Potortì. Rssi localisation with sensors placed on the user. In *2010 International Conference on Indoor Positioning and Indoor Navigation*, pages 1–6, Sept 2010.

[8] C. Beder and M. Klepal. Fingerprinting based localisation revisited: A rigorous approach for comparing rssi measurements coping with missed access points and differing antenna attenuations. In *2012 International Conference on Indoor Positioning and Indoor Navigation (IPIN)*, pages 1–7, Nov 2012.

[9] I. Borg and P. Groenen. *Modern Multidimensional Scaling: Theory and Applications*. Springer, 2005.

[10] I. Borg and J. Lingoes. *Multidimensional similarity structure analysis*. Springer, 1987.

[11] J. Borras, P. Hatrack, and N. B. Mandayam. Decision theoretic framework for nlos identification. In *Vehicular Technology Conference, 1998. VTC 98. 48th IEEE*, volume 2, pages 1583–1587 vol.2, May 1998.

[12] J. Blake Bullock, Mahesh Chowdhary, Dimitri Rubin, Donald Leimer, Greg Turetzky, and Murray Jarvis. Continuous indoor positioning using gnss, wi-fi, and mems dead reckoning. In *Proceedings of the 25th International Technical Meeting of The Satellite Division of the Institute of Navigation (ION GNSS 2012)*, pages 2408–2416, September 2012.

[13] Y. Chen, Z. Liu, X. Fu, B. Liu, and W. Zhao. Theory underlying measurement of aoa with a rotating directional antenna. In *2013 Proceedings IEEE INFOCOM*, pages 2490–2498, April 2013.

[14] Zhikui Chen, Feng Xia, Tao Huang, Fanyu Bu, and Haozhe Wang. A localization method for the internet of things. *The Journal of Supercomputing*, 63(3):657–674, Mar 2013.

[15] A. Colombo, D. Fontanelli, D. Macii, and L. Palopoli. Flexible indoor localization and tracking based on a wearable platform and sensor data fusion. *IEEE Transactions on Instrumentation and Measurement*, 63(4):864–876, April 2014.

[16] Li Cong and Weihua Zhuang. Nonline-of-sight error mitigation in mobile location. *IEEE Transactions on Wireless Communications*, 4(2):560–573, March 2005.

[17] A. J. Coulson, A. G. Williamson, and R. G. Vaughan. A statistical basis for lognormal shadowing effects in multipath fading channels. *IEEE Transactions on Communications*, 46(4):494–502, Apr 1998.

[18] A. Darif, R. Saadane, and D. Aboutajdine. An efficient short range wireless communication technology for wireless sensor network. In *2014 Third IEEE International Colloquium in Information Science and Technology (CIST)*, pages 396–401, Oct 2014.

[19] Jan de Leeuw. Convergence of the majorization method for multidimensional scaling. *Journal of Classification*, 5(2):163–180, 1988.

[20] Jan de Leeuw and Jacqueline Meulman. A special jackknife for multidimensional scaling. *Journal of Classification*, 3(1):97–112, Mar 1986.

[21] V. Dehghanian and M. Lowe. Rss-ins integration for cooperative indoor positioning. In *2016 International Conference on Indoor Positioning and Indoor Navigation (IPIN)*, pages 1–7, Oct 2016.

[22] C. Di Franco, A. Melani, and M. Marinoni. Solving ambiguities in MDS relative localization. In *2015 International Conference on Advanced Robotics (ICAR)*, pages 230–236, July 2015.

[23] L. Doherty, K. S. J. pister, and L. El Ghaoui. Convex position estimation in wireless sensor networks. In *Proceedings IEEE INFOCOM 2001. Conference on Computer Communications. Twentieth Annual Joint Conference of the IEEE Computer and Communications Society (Cat. No.01CH37213)*, volume 3, pages 1655–1663 vol.3, April 2001.

[24] Z. Dong, Y. Wu, and D. Sun. Data fusion of the real time positioning system based on rssi and tof. In *2013 5th International Conference on Intelligent Human-Machine Systems and Cybernetics*, volume 2, pages 503–506, Aug 2013.

[25] N. Le Dortz, F. Gain, and P. Zetterberg. Wifi fingerprint indoor positioning system using probability distribution comparison. In *2012 IEEE International Conference on Acoustics, Speech and Signal Processing (ICASSP)*, pages 2301–2304, March 2012.

[26] P. Drineas, A. Javed, M. Magdon-Ismail, G. Pandurangant, R. Virrankoski, and A. Savvides. Distance matrix reconstruction from incomplete distance information for sensor network localization. In *2006 3rd Annual IEEE Communications Society on Sensor and Ad Hoc Communications and Networks*, volume 2, pages 536–544, Sept 2006.

[27] V. N. Ekambaram, K. Ramchandran, and R. Sengupta. Scaling laws for cooperative node localization in non-line-of-sight wireless networks. In *2011 IEEE Global Telecommunications Conference - GLOBECOM 2011*, pages 1–5, Dec 2011.

[28] Bruno Figueira, Bruno Gonçalves, Hugo Folgado, Nerijus Masiulis, Julio Calleja-González, and Jaime Sampaio. Accuracy of a basketball indoor tracking system based on standard bluetooth low energy channels (nbn23Ž). *Sensors*, 18(6), 2018.

[29] F. Fletcher, Branko Ristic, and Darko Musicki. Recursive estimation of emitter location using tdoa measurements from two uavs. In *2007 10th International Conference on Information Fusion*, pages 1–8, July 2007.

[30] C. Di Franco, E. Bini, M. Marinoni, and G. C. Buttazzo. Multidimensional scaling localization with anchors. In *2017 IEEE International Conference on Autonomous Robot Systems and Competitions (ICARSC)*, pages 49–54, April 2017.

[31] M. Gadd and P. Newman. A framework for infrastructure-free warehouse navigation. In *2015 IEEE International Conference on Robotics and Automation (ICRA)*, pages 3271–3278, May 2015.

[32] A. Galov, A. Moschevikin, and R. Voronov. Combination of rss localization and tof ranging for increasing positioning accuracy indoors. In *2011 11th International Conference on ITS Telecommunications*, pages 299–304, Aug 2011.

[33] W. A. Gardner and C. . Chen. Signal-selective time-difference-of-arrival estimation for passive location of man-made signal sources in highly corruptive environments. i. theory and method. *IEEE Transactions on Signal Processing*, 40(5):1168–1184, May 1992.

[34] L. Gogolak, S. Pletl, and D. Kukolj. Indoor fingerprint localization in wsn environment based on neural network. In *2011 IEEE 9th International Symposium on Intelligent Systems and Informatics*, pages 293–296, Sept 2011.

[35] J. R. Gonzalez and C. J. Bleakley. High-precision robust broadband ultrasonic location and orientation estimation. *IEEE Journal of Selected Topics in Signal Processing*, 3(5):832–844, Oct 2009.

[36] E. Le Grand and S. Thrun. 3-axis magnetic field mapping and fusion for indoor localization. In *2012 IEEE International Conference on Multisensor Fusion and Integration for Intelligent Systems (MFI)*, pages 358–364, Sept 2012.

[37] Louis Guttman. A general nonmetric technique for finding the smallest coordinate space for a configuration of points. *Psychometrika*, 33(4):469–506, Dec 1968.

[38] I. Guvenc, C. C. Chong, and F. Watanabe. Nlos identification and mitigation for uwb localization systems. In *2007 IEEE Wireless Communications and Networking Conference*, pages 1571–1576, March 2007.

[39] İsmail Güvenç, Chia-Chin Chong, Fujio Watanabe, and Hiroshi Inamura. Nlos identification and weighted least-squares localization for uwb systems using multipath channel statistics. *EURASIP Journal on Advances in Signal Processing*, 2008(1):271984, Aug 2007.

[40] T. Gädeke, J. Schmid, M. Krüger, J. Jany, W. Stork, and K. D. Müller-Glaser. A bi-modal ad-hoc localization scheme for wireless networks based on rss and tof fusion. In *2013 10th Workshop on Positioning, Navigation and Communication (WPNC)*, pages 1–6, March 2013.

[41] H. Hashemi. The indoor radio propagation channel. *Proceedings of the IEEE*, 81(7):943–968, Jul 1993.

[42] M. Heidari, F. O. Akgul, N. A. Alsindi, and K. Pahlavan. Neural network assisted identification of the absence of direct path in indoor localization. In *IEEE GLOBECOM 2007 - IEEE Global Telecommunications Conference*, pages 387–392, Nov 2007.

[43] M. Heidari, F. O. Akgul, and K. Pahlavan. Identification of the absence of direct path in indoor localization systems. In *2007 IEEE 18th International Symposium on Personal, Indoor and Mobile Radio Communications*, pages 1–6, Sept 2007.

[44] K. Heurtefeux and F. Valois. Is rssi a good choice for localization in wireless sensor network? In *2012 IEEE 26th International Conference on Advanced Information Networking and Applications*, pages 732–739, March 2012.

[45] S. Holm. Ultrasound positioning based on time-of-flight and signal strength. In *2012 International Conference on Indoor Positioning and Indoor Navigation (IPIN)*, pages 1–6, Nov 2012.

[46] A. K. M. M. Hossain and W. S. Soh. A comprehensive study of bluetooth signal parameters for localization. In *2007 IEEE 18th International Symposium on Personal, Indoor and Mobile Radio Communications*, pages 1–5, Sept 2007.

[47] M. G. Jadidi, M. Patel, and J. V. Miro. Gaussian processes online observation classification for rssi-based low-cost indoor positioning systems. In *2017 IEEE International Conference on Robotics and Automation (ICRA)*, pages 6269–6275, May 2017.

[48] A. A. Kannan, Guoqiang Mao, and B. Vucetic. Simulated annealing based localization in wireless sensor network. In *The IEEE Conference on Local Computer Networks 30th Anniversary (LCN'05)l*, pages 2 pp.–514, Nov 2005.

[49] Wei-Wen Kao. Integration of gps and dead-reckoning navigation systems. In *Vehicle Navigation and Information Systems Conference, 1991*, volume 2, pages 635–643, Oct 1991.

[50] T. C. Karalar and J. Rabaey. An rf tof based ranging implementation for sensor networks. In *2006 IEEE International Conference on Communications*, volume 7, pages 3347–3352, June 2006.

[51] M. Kleinert and S. Schleith. Inertial aided monocular slam for gps-denied navigation. In *2010 IEEE Conference on Multisensor Fusion and Integration*, pages 20–25, Sept 2010.

[52] R. Klukas and M. Fattouche. Line-of-sight angle of arrival estimation in the outdoor multipath environment. *IEEE Transactions on Vehicular Technology*, 47(1):342–351, Feb 1998.

[53] M. Koledoye. Experiments and samples in multidimensional scaling. `https://github.com/lab-robotics-unipv/mds_experiments`, 2018 (accessed October 1, 2018).

[54] M. Koledoye. Experiments in mds with nlos mitigation. `https://github.com/lab-robotics-unipv/MDS-NLOS-mitigation`, 2018 (accessed October 15, 2018).

[55] Manikanta Kotaru, Kiran Joshi, Dinesh Bharadia, and Sachin Katti. Spotfi: Decimeter level localization using wifi. In *Proceedings of the 2015 ACM Conference on Special Interest Group on Data Communication*, SIGCOMM '15, pages 269–282, New York, NY, USA, 2015. ACM.

[56] A. S. Krishnakumar and P. Krishnan. On the accuracy of signal strength-based estimation techniques. In *Proceedings IEEE 24th Annual Joint Conference of the IEEE Computer and Communications Societies.*, volume 1, pages 642–650 vol. 1, March 2005.

[57] M. Kuhn, C. Zhang, B. Merkl, D. Yang, Y. Wang, M. Mahfouz, and A. Fathy. High accuracy uwb localization in dense indoor environments. In *2008 IEEE*

International Conference on Ultra-Wideband, volume 2, pages 129–132, Sept 2008.

[58] J. Lee, Y. Su, and C. Shen. A comparative study of wireless protocols: Bluetooth, uwb, zigbee, and wi-fi. In *IECON 2007 - 33rd Annual Conference of the IEEE Industrial Electronics Society*, pages 46–51, Nov 2007.

[59] Jan De Leeuw, In J. R. Barra, F. Brodeau, G. Romier, and B. Van Cutsem (eds.). Applications of convex analysis to multidimensional scaling. In *Recent Developments in Statistics*, pages 133–146. North Holland Publishing Company, 1977.

[60] Q. Li, W. Li, W. Sun, J. Li, and Z. Liu. Fingerprint and assistant nodes based wi-fi localization in complex indoor environment. *IEEE Access*, 4:2993–3004, 2016.

[61] Xiaoli Li, Hongchi Shi, and Yi Shang. Sensor network localisation based on sorted rssi quantisation. *Int. J. Ad Hoc Ubiquitous Comput.*, 1(4):222–229, July 2006.

[62] D. Lymberopoulos and J. Liu. The microsoft indoor localization competition: Experiences and lessons learned. *IEEE Signal Processing Magazine*, 34(5):125–140, Sept 2017.

[63] D. Macii, F. Trenti, and P. Pivato. A robust wireless proximity detection technique based on rss and tof measurements. In *2011 IEEE International Workshop on Measurements and Networking Proceedings (M N)*, pages 31–36, Oct 2011.

[64] A. Mannesson, M. A. Yaqoob, F. Tufvesson, and B. Bernhardsson. Radio and imu based indoor positioning and tracking. In *2012 19th International Conference on Systems, Signals and Image Processing (IWSSIP)*, pages 32–35, April 2012.

[65] Guoqiang Mao, Baris Fidan, Guoqiang Mao, and Baris Fidan. *Localization Algorithms and Strategies for Wireless Sensor Networks*. Information Science Reference - Imprint of: IGI Publishing, Hershey, PA, 2009.

[66] Apostolos Meliones and Demetrios Sampson. Blind museumtourer: A system for self-guided tours in museums and blind indoor navigation. *Technologies*, 6(1), 2018.

[67] P. Mirowski, H. Steck, P. Whiting, R. Palaniappan, M. MacDonald, and T. K. Ho. Kl-divergence kernel regression for non-gaussian fingerprint based localization. In *2011 International Conference on Indoor Positioning and Indoor Navigation*, pages 1–10, Sept 2011.

[68] N. P. M. Y. Nayan, M. F. Hassan, and F. Subhan. Filters for device-free indoor localization system based on rssi measurement. In *2014 International Conference on Computer and Information Sciences (ICCOINS)*, pages 1–5, June 2014.

[69] D. Niculescu and B. Nath. Ad hoc positioning system (aps). In *GLOBECOM'01. IEEE Global Telecommunications Conference (Cat. No.01CH37270)*, volume 5, pages 2926–2931 vol.5, Nov 2001.

[70] J. Niu, B. Wang, L. Cheng, and J. J. P. C. Rodrigues. Wicloc: An indoor localization system based on wifi fingerprints and crowdsourcing. In *2015 IEEE International Conference on Communications (ICC)*, pages 3008–3013, June 2015.

[71] L. Oliveira, L. Almeida, and P. Lima. Multi-hop routing within tdma slots for teams of cooperating robots. In *2015 IEEE World Conference on Factory Communication Systems (WFCS)*, pages 1–8, May 2015.

[72] L. Oliveira, C. Di Franco, T. E. Abrudan, and L. Almeida. Fusing time-of-flight and received signal strength for adaptive radio-frequency ranging. In *2013 16th International Conference on Advanced Robotics (ICAR)*, pages 1–6, Nov 2013.

[73] Ian Oppermann, Matti Hämäläinen, and Jari Iinatti. *UWB: theory and applications*. John Wiley & Sons, 2005.

[74] N. Patwari, J. N. Ash, S. Kyperountas, A. O. Hero, R. L. Moses, and N. S. Correal. Locating the nodes: cooperative localization in wireless sensor networks. *IEEE Signal Processing Magazine*, 22(4):54–69, July 2005.

[75] N. Patwari, A. O. Hero, M. Perkins, N. S. Correal, and R. J. O'Dea. Relative location estimation in wireless sensor networks. *IEEE Transactions on Signal Processing*, 51(8):2137–2148, Aug 2003.

[76] A. S. Paul and E. A. Wan. Rssi-based indoor localization and tracking using sigma-point kalman smoothers. *IEEE Journal of Selected Topics in Signal Processing*, 3(5):860–873, Oct 2009.

[77] C. Perey and T. Miyashita. Indoor positioning and navigation for mobile ar. In *2011 IEEE International Symposium on Mixed and Augmented Reality - Arts, Media, and Humanities*, pages 1–1, Oct 2011.

[78] M. J. D. Powell. An efficient method for finding the minimum of a function of several variables without calculating derivatives. *The Computer Journal*, 7(2):155–162, 1964.

[79] Yihong Qi and H. Kobayashi. On relation among time delay and signal strength based geolocation methods. In *Global Telecommunications Conference, 2003. GLOBECOM '03. IEEE*, volume 7, pages 4079–4083 vol.7, Dec 2003.

[80] C. Radhakrishna Rao. Information and the accuracy attainable in the estimation of statistical parameters. *Bull. Calcutta Math. Soc.*, 37:81–91, 1945.

[81] C. Röhrig and M. Müller. Indoor location tracking in non-line-of-sight environments using a ieee 802.15.4a wireless network. In *2009 IEEE/RSJ International Conference on Intelligent Robots and Systems*, pages 552–557, Oct 2009.

[82] U. Schatzberg, L. Banin, and Y. Amizur. Enhanced wifi tof indoor positioning system with mems-based ins and pedometric information. In *Record - IEEE PLANS, Position Location and Navigation Symposium*, pages 185–192, 2014. Cited By :12.

[83] Stephan V Schell and William A Gardner. High-resolution direction finding.

[84] Yi Shang and W. Ruml. Improved mds-based localization. In *IEEE INFOCOM 2004*, volume 4, pages 2640–2651 vol.4, March 2004.

[85] Yi Shang, Wheeler Ruml, Ying Zhang, and Markus P. J. Fromherz. Localization from mere connectivity. In *Proceedings of the 4th ACM International Symposium on Mobile Ad Hoc Networking &Amp; Computing*, MobiHoc '03, pages 201–212, New York, NY, USA, 2003. ACM.

[86] Yi Shang, Hongchi Shi, and A. A. Ahmed. Performance study of localization methods for ad-hoc sensor networks. In *2004 IEEE International Conference on Mobile Ad-hoc and Sensor Systems (IEEE Cat. No.04EX975)*, pages 184–193, Oct 2004.

[87] A. Sheinker, B. Ginzburg, N. Salomonski, L. Frumkis, and B. Kaplan. Localization in 2d using beacons of low frequency magnetic field. *IEEE Journal of*

Selected Topics in Applied Earth Observations and Remote Sensing, 6(2):1020–1030, April 2013.

[88] W. Shi and V. W. S. Wong. Mds-based localization algorithm for rfid systems. In *2011 IEEE International Conference on Communications (ICC)*, pages 1–6, June 2011.

[89] S. P. Subramanian, J. Sommer, S. Schmitt, and W. Rosenstiel. Sbil: Scalable indoor localization and navigation service. In *2007 Third International Conference on Wireless Communication and Sensor Networks*, pages 27–30, Dec 2007.

[90] Lixin Tang and S. Yuta. Vision based navigation for mobile robots in indoor environment by teaching and playing-back scheme. In *Proceedings 2001 ICRA. IEEE International Conference on Robotics and Automation (Cat. No.01CH37164)*, volume 3, pages 3072–3077 vol.3, May 2001.

[91] J. Tiemann and C. Wietfeld. Scalable and precise multi-uav indoor navigation using tdoa-based uwb localization. In *2017 International Conference on Indoor Positioning and Indoor Navigation (IPIN)*, pages 1–7, Sept 2017.

[92] T. Ussmueller, D. Brenk, J. Essel, J. Heidrich, G. Fischer, and R. Weigel. Roundtrip-time-of-flight based localization of passive multi-standard rfid-tags. In *2012 IEEE International Conference on Wireless Information Technology and Systems (ICWITS)*, pages 1–4, Nov 2012.

[93] S. Venkatesh and R. M. Buehrer. Non-line-of-sight identification in ultra-wideband systems based on received signal statistics. *IET Microwaves, Antennas Propagation*, 1(6):1120–1130, Dec 2007.

[94] David J. Wales and Jonathan P. K. Doye. Global optimization by basin-hopping and the lowest energy structures of lennard-jones clusters containing up to 110 atoms. *The Journal of Physical Chemistry A*, 101(28):5111–5116, 1997.

[95] Q. Wang, H. Luo, F. Zhao, and W. Shao. An indoor self-localization algorithm using the calibration of the online magnetic fingerprints and indoor landmarks. In *2016 International Conference on Indoor Positioning and Indoor Navigation (IPIN)*, pages 1–8, Oct 2016.

[96] A. Ward, A. Jones, and A. Hopper. A new location technique for the active office. *IEEE Personal Communications*, 4(5):42–47, Oct 1997.

[97] Wang Wei, Xiong Jin-Yu, and Zhu Zhong-Liang. A new NLOS error mitigation algorithm in location estimation. *IEEE Transactions on Vehicular Technology*, 54(6):2048–2053, Nov 2005.

[98] A. J. Weiss. On the accuracy of a cellular location system based on rss measurements. *IEEE Transactions on Vehicular Technology*, 52(6):1508–1518, Nov 2003.

[99] Y. Wen, X. Tian, X. Wang, and S. Lu. Fundamental limits of rss fingerprinting based indoor localization. In *2015 IEEE Conference on Computer Communications (INFOCOM)*, pages 2479–2487, April 2015.

[100] M. Z. Win, R. A. Scholtz, and M. A. Barnes. Ultra-wide bandwidth signal propagation for indoor wireless communications. In *Proceedings of ICC'97 - International Conference on Communications*, volume 1, pages 56–60 vol.1, June 1997.

[101] M. A. Youssef, A. Agrawala, and A. Udaya Shankar. Wlan location determination via clustering and probability distributions. In *Proceedings of the First IEEE International Conference on Pervasive Computing and Communications, 2003. (PerCom 2003).*, pages 143–150, March 2003.

[102] K. Yu and Y. J. Guo. Improved positioning algorithms for nonline-of-sight environments. *IEEE Transactions on Vehicular Technology*, 57(4):2342–2353, July 2008.

[103] K. Yu and Y. J. Guo. Non-line-of-sight detection based on toa and signal strength. In *2008 IEEE 19th International Symposium on Personal, Indoor and Mobile Radio Communications*, pages 1–5, Sept 2008.

[104] K. Yu and Y. J. Guo. Statistical nlos identification based on aoa, toa, and signal strength. *IEEE Transactions on Vehicular Technology*, 58(1):274–286, Jan 2009.

[105] F. Zampella, A. R. Jiménez Ruiz, and F. Seco Granja. Indoor positioning using efficient map matching, rss measurements, and an improved motion model. *IEEE Transactions on Vehicular Technology*, 64(4):1304–1317, April 2015.

[106] A. Zanella. Best practice in rss measurements and ranging. *IEEE Communications Surveys Tutorials*, 18(4):2662–2686, Fourthquarter 2016.

[107] J. Zhang, J. Sun, H. Wang, W. Xiao, and L. Tan. Large-scale wifi indoor localization via extreme learning machine. In *2017 36th Chinese Control Conference (CCC)*, pages 4115–4120, July 2017.

[108] Kaibi Zhang, Yangchuan Zhang, and Subo Wan. Research of rssi indoor ranging algorithm based on gaussian - kalman linear filtering. In *2016 IEEE Advanced Information Management, Communicates, Electronic and Automation Control Conference (IMCEC)*, pages 1628–1632, Oct 2016.

[109] Rui Zhang, Weiwei Xia, Ziyan Jia, and Lianfeng Shen. The indoor localization method based on the integration of rssi and inertial sensor. In *2014 IEEE 3rd Global Conference on Consumer Electronics (GCCE)*, pages 332–336, Oct 2014.

[110] H. Zhou and N. N. Van. Indoor fingerprint localization based on fuzzy c-means clustering. In *2014 Sixth International Conference on Measuring Technology and Mechatronics Automation*, pages 337–340, Jan 2014.